

We and other groups have shown that the histone acetyltransferase (HAT) TIP60/Esal participates in the DNA damage response as a protein complex (9, 13, 16, 30, 54, 55). For example, TIP60 induces histone H4 acetylation and the accumulation of repair molecules, including RAD51, at sites of DSBs with TRRAP in human cells (30). In *Saccharomyces cerevisiae*, the NuA4 complex, including Esal, a yeast homologue of human TIP60, binds histone H4 through Arp4 to mediate the DSB-induced acetylation of H4 (9). However, it is not yet known how histone acetylation by the TIP60 complex regulates chromatin organization immediately after the induction of DSBs in the human DNA repair response.

In addition to histone modifications, histone eviction/release and histone variant exchange can facilitate DNA repair by recruiting signaling and repair factors (12, 25, 57). The exchange of core histones for a specific variant within nucleosomes can also alter chromatin structure in a temporally controlled manner (1, 3, 19, 22, 26, 28, 42, 49, 62). For example, *Drosophila melanogaster* DmTIP60 has been shown to acetylate phospho-H2A.v in vitro, resulting in its removal from chromatin due to exchange with an unmodified H2A.v (22). In budding yeast, H2A (or phospho-H2A) is replaced with the H2A variant Htz1 by the histone exchange complex SWR1 (28). The INO80 complex provokes chromatin reorganization following DNA damage; this reorganization includes the release of histones H2B and H3 at sites around DSBs, leading to the recruitment of RAD51 (29, 53). Furthermore, the histone variant H3.1 appears to be deposited at sites of UV damage by the chromatin assembly factor CAF-1 (36). Although these studies indicate that histone eviction and variant exchange are important mechanisms for altering chromatin structure during the DNA damage response (35, 57), it is not clear how histone modifications engage in these chromatin reorganizations immediately following the induction of DSBs during DNA repair in human cells.

Here, we show that the TIP60 HAT complex interacts with H2AX immediately after exposure to ionizing irradiation (IR). Furthermore, DSBs facilitate the association of TIP60 with the ubiquitin-conjugating enzyme UBC13 (2). The TIP60-UBC13 complex regulates the acetylation and ubiquitination of H2AX following the formation of DSBs. The DSB-induced acetylation of H2AX lysine 5 (K5) is required for this ubiquitination and occurs independently of the phosphorylation of H2AX. We also show that damage-induced acetylation and ubiquitination provoke the release of H2AX from chromatin immediately after the induction of DSBs. Because TIP60-UBC13 is required for the DSB-induced ubiquitination and release of H2AX, these findings provide the first evidence that human TIP60 promotes the acetylation-dependent ubiquitination of H2AX by UBC13, causing H2AX release from chromatin, which facilitates chromatin reorganization following DNA damage.

#### MATERIALS AND METHODS

**Cell culture.** HeLa cells (16) (kind gift from Y. Nakatani, Dana-Faber Cancer Institute) and GM02063 (51), a simian virus 40-transformed human fibroblast cell line, were cultured in Dulbecco's modified Eagle's medium supplemented with 10% fetal calf serum.

**Reagents and antibodies.** Anti-FLAG and antihemagglutinin (anti-HA) antibody-conjugated agaroses (Sigma) were used for the purification of FLAG-HA-

tagged proteins. Immunoblotting analyses were performed with anti-TIP60 (Upstate), anti-acetylated H2A(K5) (Cell Signaling), anti-glyceraldehyde-3-phosphate dehydrogenase (anti-GAPDH) (Santa Cruz Biotechnology), anti-FLAG (Sigma), anti-H2AX (Sigma), antiubiquitin (FK2; Nippon Bio-Test Lab), anti-UBC13 (Zymed), and anti-HA (Roche) antibodies.

**Affinity purification of H2AX and TIP60 complexes.** HeLa cells expressing FLAG-HA epitope-tagged H2AX (eH2AX; wild type or site-specific mutants) or TIP60 (eTIP60) were grown to  $1.0 \times 10^6$  cells/ml as suspension cultures. For the induction of DNA damage, cells were  $\gamma$ -irradiated (12 Gy) after centrifugation. The nuclear extract and chromatin fraction were prepared from the cells, and the H2AX and TIP60 complexes were purified from the nuclear extracts as previously described (16, 31). To affinity purify eH2AX (wild type and mutants) from the chromatin fraction, the nuclear pellet was resuspended in a buffer of 20 mM Tris-HCl (pH 8.0), 500 mM KCl, 5 mM MgCl<sub>2</sub>, 0.2 mM EDTA, 10% glycerol, 0.1% Tween 20, 10 mM 2-mercaptoethanol, and 0.25 mM phenylmethylsulfonyl fluoride and then lysed by sonication. After the removal of insoluble material by centrifugation, eH2AX and eTIP60 were affinity purified (16, 31).

**Microirradiation, FRAP, and iFRAP.** GM02063 cells expressing green fluorescent protein (GFP)-tagged H2AX (GFP-H2AX; wild type or site-specific mutants), H2A (GFP-H2A), H2B (GFP-H2B), H3 (GFP-H3), or H4 (GFP-H4) were maintained on the microscope stage in an FCS live-cell chamber system (Biopatch) at 37°C. Imaging, microirradiation, and fluorescence recovery after photobleaching (FRAP) experiments were performed using an LSM510 confocal microscope (Carl Zeiss). For microirradiation, sensitization of cells was performed by incubating the cells for 20 h in medium containing 2.5  $\mu$ M deoxyribosylthymine and 0.3  $\mu$ M bromodeoxyuridine (Sigma) and then staining with 2  $\mu$ g/ml Hoechst 33258 (Sigma) for 10 min before UVA microirradiation as described previously (58). The 364-nm line of the UVA laser was used for microirradiation (three pulses at 180  $\mu$ W). The maximum power of the 488-nm Ar laser line was used for photobleaching in FRAP analysis. For imaging, the laser was attenuated to 0.1%. For inverse FRAP (iFRAP) experiments (14, 37), photobleaching was performed under the same conditions as for FRAP analysis. All fluorescence regions except for small regions in irradiated and unirradiated areas were bleached, and the remaining GFP fluorescence was chased using the LSM510 confocal microscope. For FRAP and iFRAP analysis, a prebleached image was acquired just after the induction of DSBs by UVA laser microirradiation, after which the bleaching pulse was delivered. To quantify fluorescence recovery, single optical sections were collected at 3- or 5-s intervals for the indicated periods of time. Image J was used for the quantification of fluorescent intensity in FRAP analysis. Background fluorescence intensity (BG) was measured in a random field outside of the cells. The average fluorescence intensity in the bleached region at each time point ( $I_t$ ) was measured in a region corresponding to at least 30% of the bleached region. For each time point, the relative intensity was calculated as follows:  $I_{rel,t} = (I_t - BG)/(I_0 - BG)$ , where  $I_0$  is the average intensity of the region before bleaching. The percent recovery after 260 s in FRAP analysis ( $P_{recovery;260s}$ ) was calculated as follows:  $P_{recovery;260s} = 100 \times (I_{rel;260s} - I_{rel;6s})/(1 - I_{rel;6s})$ , where  $I_{rel;6s}$  is the relative intensity of the bleached area in the first image taken after bleaching (6 s after bleaching), and  $I_{rel;260s}$  is the relative intensity of the bleached area in the image taken 260 s after bleaching. Statistical comparisons were made using Student's *t* test. Image J was also used to generate profile plots of fluorescence intensity in the iFRAP analysis.

**Immunofluorescence analysis.** Cells were fixed with 4% paraformaldehyde in  $1 \times$  phosphate-buffered saline (PBS). Next, nuclei were permeabilized with 0.1% sodium dodecyl sulfate (SDS)-0.5% Triton X-100 in  $1 \times$  PBS for 5 min. An in situ cell death detection kit (Roche) was used for the terminal deoxynucleotidyltransferase-mediated dUTP-biotin nick end labeling (TUNEL) technique as recommended by the manufacturer. For the detection of RAD51, fixed cells were incubated for 30 min at 37°C with anti-RAD51 antibody (1:2,000; kindly provided by A. Shinohara, Osaka University) in 1% bovine serum albumin- $1 \times$  PBS. Fluorescein isothiocyanate-conjugated goat anti-rabbit (1:1,000; Biosource) was used as the secondary antibody. Nuclei were stained with Hoechst 33342. Samples were examined with an Axioplan2 microscope and using an AxioCam MRm controlled by Axiovision (Zeiss).

**MS-MS analysis.** Protein sequences were determined using an ultraflex time-of-flight mass spectrometer (Bruker Daltonics) equipped with a nitrogen laser operating at 337 nm. The samples were also examined by tandem mass spectrometry (MS-MS) methods with an AXIMA-QIT (Shimadzu-Kratos) ion trap matrix-assisted laser desorption mass spectrometry (MS). The following sequences were extracted: for TIP60, N'-EVPASQASGK-C', N'-LFYVHYDFNK-C', N'-LLIEFSYELSKVEGK-C', and N'-EDVISTLQYLNLNLYYK-C'; for Ub-H2AX, N'-AGLQFPVGR-C', N'-ESTLHLVLR-C', N'-K(LRGG)TSATVGPK-C', and

N'-HLQLAIRNDEELN-C'; and for H2AX, N'-HLQLAIR-C', N'-AGLQFPVGR-C', and N'-LLGGVTIAQGGVLPNIQAVLLPK-C'.

**siRNA.** The short interfering RNA (siRNA) expression vector pSUPER.retro.puro (OligoEngine) was used to knock down TIP60 (target sequence, 5'-GGACATCAGTGGCCGGAAGC-3' [siTIP60.1] or 5'-ACGGAAGGTGGA GGTGGT-3' [siTIP60.2]), H2AX (5'-CTGGAATTCTGCAGCTAAC-3'), or UBC13 (5'-AAGCATGAGCAGAGGCTAGAA-3' [siUBC13.1] or 5'-AAGCA GCTAACCAAGGTCTTTA-3' [siUBC13.2]). Retroviral production was used to generate GM02063 cells or HeLa cells stably expressing TIP60-, H2AX-, and UBC13-specific or control siRNAs based on puromycin resistance. To measure the levels of proteins, cells were lysed in protein sample buffer and analyzed by immunoblotting.

## RESULTS

**TIP60 HAT regulates DNA damage-induced acetylation of H2AX.** To identify proteins that associate with H2AX immediately after the induction of DNA damage, stably expressed FLAG-HA eH2AX was purified from nuclear extracts of HeLa cells following treatment with IR. Purification of eH2AX was performed by sequential steps of affinity chromatography on anti-FLAG antibody-conjugated agarose followed by anti-HA antibody-conjugated agarose (16, 31), and the associated proteins were analyzed by SDS-polyacrylamide gel electrophoresis. SDS-polyacrylamide gel electrophoresis analysis of the purified H2AX complexes indicated that several proteins are associated with H2AX in a DNA damage-dependent manner (see Fig. S1A in the supplemental material). We employed MS analysis to identify the binding partner of H2AX. MS analysis indicated that TIP60 HAT was included in the purified H2AX complex following the induction of DNA damage by IR. This was confirmed by immunoblotting with an anti-TIP60 antibody (Fig. 1A). In contrast, a similar analysis of H2A-binding proteins from irradiated cells did not show the presence of TIP60 (Fig. 1A). These findings suggest that TIP60 interacts specifically with H2AX in the nuclear soluble fraction after IR.

Previous studies have shown that K5 of histone H2A is acetylated by TIP60 *in vitro* (18). Because the K5 site is well conserved between H2AX and H2A, we examined K5 acetylation in immunoaffinity-purified H2AX by immunoblotting analysis using an anti-acetyl-H2A(K5) antibody. We found that H2AX(K5) was acetylated and that the amount of acetylated H2AX (Ac-H2AX) was substantially increased by IR (Fig. 1B). This finding was confirmed by MS-MS analysis (data not shown).

To confirm the role of TIP60 in H2AX acetylation, we constructed human GM02063 fibroblasts (51) that stably express TIP60 siRNA. In these cells, the amount of TIP60 protein was reduced by >80% (Fig. 1C). We then transiently transfected the cells with FLAG-H2AX, treated them with and without IR, and performed immunoprecipitation using an anti-FLAG antibody. Immunoblotting indicated that the DSB-induced acetylation of H2AX(K5) was significantly suppressed in TIP60 siRNA-expressing cells (Fig. 1D). Similar results were obtained using another TIP60-specific siRNA, confirming that the suppression of H2AX(K5) acetylation was due to the specific depletion of TIP60 (see Fig. S2A and B in the supplemental material). Moreover, the TIP60 complex directly acetylated free H2AX and H2AX in a nucleosomal context *in vitro* (data not shown). These results suggest that TIP60 is required for the acetylation of H2AX(K5) in the very early stages of the DNA damage response.

We next confirmed the DSB-induced interaction between H2AX and TIP60 by reciprocal affinity purification experiments using HeLa cells expressing FLAG-HA eTIP60. The TIP60 complex purified from the nuclear soluble fraction of irradiated cells included endogenous H2AX (Fig. 1E). Interestingly, immunoblot analysis using an anti-H2AX antibody revealed multiple higher-molecular-weight bands in addition to the band corresponding to H2AX. This finding indicated that TIP60-associated H2AX may contain modifications other than acetylation and phosphorylation following IR-induced DNA damage (Fig. 1E).

**Acetylation by TIP60 is required for the ubiquitination of H2AX following DNA damage.** The approximate molecular weight differences of the slower-migrating species led us to speculate that H2AX in the nuclear soluble fraction is polyubiquitinated upon DSBs. Immunoblotting of purified eH2AX from the soluble nuclear fraction revealed that multiple bands reacted with both anti-H2AX and antiubiquitin antibodies following IR (Fig. 2A). MS-MS analysis confirmed that the ~32-kDa protein was a form of eH2AX ubiquitinated on lysine 119 [Ub-eH2AX(K119)] (see Fig. S1B in the supplemental material). The DNA damage-dependent polyubiquitination of H2AX on K119 was further confirmed by eH2AX in which K119 was replaced with Arg [eH2AX(K119R)]. As expected, the DSB-induced polyubiquitination of eH2AX was significantly suppressed in eH2AX(K119R) mutant-expressing HeLa cells by immunoblotting analysis using anti-H2AX and antiubiquitin (FK2) antibodies (Fig. 2A). These results suggest that DSBs induce the polyubiquitination of H2AX at K119 in the nuclear soluble fraction of HeLa cells.

Because the TIP60 complex interacted with polyubiquitinated H2AX (poly-Ub-H2AX) after IR, we next examined the involvement of TIP60 in the polyubiquitination of H2AX in the nuclear soluble fraction. The specific depletion of TIP60 significantly suppressed the IR-induced polyubiquitination of eH2AX purified from the nuclear soluble fraction (Fig. 2A). We then analyzed whether TIP60 regulates the polyubiquitination of H2AX via the acetylation of K5 upon DNA damage. We expressed an eH2AX in which K5 was replaced with Arg [eH2AX(K5R)] in HeLa cells and then purified it by immunoaffinity chromatography from the nuclear soluble fraction of HeLa cells following treatment with or without IR. Immunoblotting analysis using anti-H2AX and antiubiquitin (FK2) antibodies revealed little or no increase in the level of polyubiquitinated eH2AX(K5R) after IR (Fig. 2A), suggesting that the DSB-induced polyubiquitination of H2AX in the nuclear soluble fraction requires TIP60-dependent acetylation.

The finding that TIP60 specifically interacts with H2AX and regulates its polyubiquitination in the nuclear soluble fraction following DNA damage suggests two possibilities. One is that TIP60 interacts with H2AX released from chromatin upon DNA damage. The other is that TIP60 is targeted to damaged chromatin and regulates the release of H2AX via histone modifications. To determine which of these possibilities is correct, we analyzed whether TIP60 regulates these H2AX modifications in the chromatin fraction. First, to examine the ubiquitination status of H2AX in the chromatin fraction, we performed anti-H2AX immunoblotting of the affinity-purified eH2AX from the chromatin fraction following treatment with or without IR. We found that eH2AX in the chromatin-bound

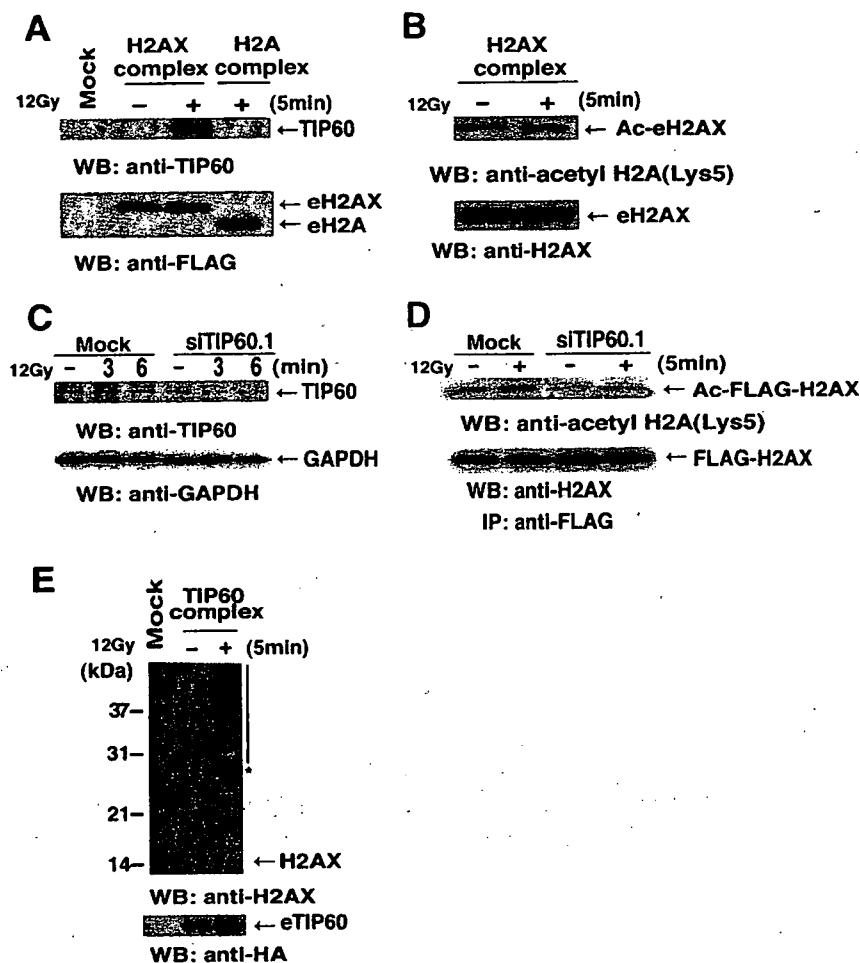


**FIG. 1.** TIP60 regulates the acetylation of H2AX(K5) upon DNA damage. (A) The mock control, eH2AX, and eH2A complexes were immunoaffinity purified from the nuclear soluble fraction of HeLa cells treated without (–) or with (+) IR at 12 Gy followed by a 5-min recovery. Immunoblotting analysis was performed with anti-TIP60 (top) and anti-FLAG (bottom) antibodies. (B) The eH2AX complex immunoaffinity purified from the nuclear soluble fraction of HeLa cells treated with IR (12 Gy) followed by a 5-min recovery. Proteins were analyzed by immunoblotting using anti-acetyl-K5 of H2A antibody (top). Unirradiated cells (–) were used as controls. eH2AX was used as a loading control (bottom). (C) Depletion of TIP60 by TIP60 siRNA. Shown are anti-TIP60 immunoblots of lysates from TIP60 siRNA (siTIP60.1)-expressing and mock control cells prepared at the indicated times after IR at 12 Gy (top). GAPDH was used as a loading control (bottom). (D) Effect of the depletion of TIP60 on the acetylation of H2AX after IR. TIP60-specific siRNA (siTIP60.1)-expressing and mock control cells transfected with a FLAG-H2AX expression vector were treated with IR at 12 Gy and allowed to recover for 5 min. Immunoprecipitation was carried out using the anti-FLAG antibody, and proteins were analyzed by immunoblotting with antibodies against H2A acetylated on K5 (top) or total H2AX (bottom). Cells were treated with sodium butyrate (final concentration, 5 mM) for the detection of acetylation. (E) Western blot analysis of the TIP60 complex by use of anti-H2AX (top) and anti-HA (bottom; loading control) antibodies. Shown are the mock control and the TIP60 complex immunoaffinity purified from nuclear extract of HeLa cells stably expressing FLAG-HA eTIP60 with IR at 12 Gy followed by a 5-min recovery. Bands that reacted with anti-H2AX antibody are indicated by an asterisk and a bar. eTIP60 was used as a loading control (bottom). WB, Western blot.

fraction was monoubiquitinated under normal conditions, as reported previously (Fig. 2B and C) (61). The level of monoubiquitination of eH2AX was increased following IR (Fig. 2B and C). Importantly, eH2AX was significantly polyubiquitinated following IR (Fig. 2C). The DSB-induced poly- and monoubiquitination of eH2AX in the chromatin fraction were abolished by the K119R mutation [eH2AX(K119R)] (Fig. 2B and C). We further confirmed these findings by a coimmunoprecipitation (coIP) experiment using 293T cells expressing FLAG-tagged H2AX(K119R) and HA-tagged ubiquitin (see Fig. S3A in the supplemental material). These results indicate that eH2AX in the chromatin fraction was mono- and polyubiquitinated at K119 following IR. However, we cannot ex-

clude the possibility that H2AX is also ubiquitinated independent of DNA damage at a residue other than K119, because a longer exposure of the anti-H2AX immunoblot of the K119R mutant suggested weak monoubiquitination after IR.

We next examined the involvement of TIP60 in the DSB-induced modifications of H2AX in the chromatin fraction. The depletion of TIP60 in HeLa cells by use of TIP60 siRNA repressed the DSB-induced mono- and polyubiquitination of eH2AX (Fig. 2C). Monoubiquitination of eH2AX and H2AX in the chromatin fraction under normal conditions was not disturbed by the depletion of TIP60 (Fig. 2C). These findings are consistent with the notion that TIP60 regulates the DSB-induced mono- and polyubiquitination of H2AX in the chro-

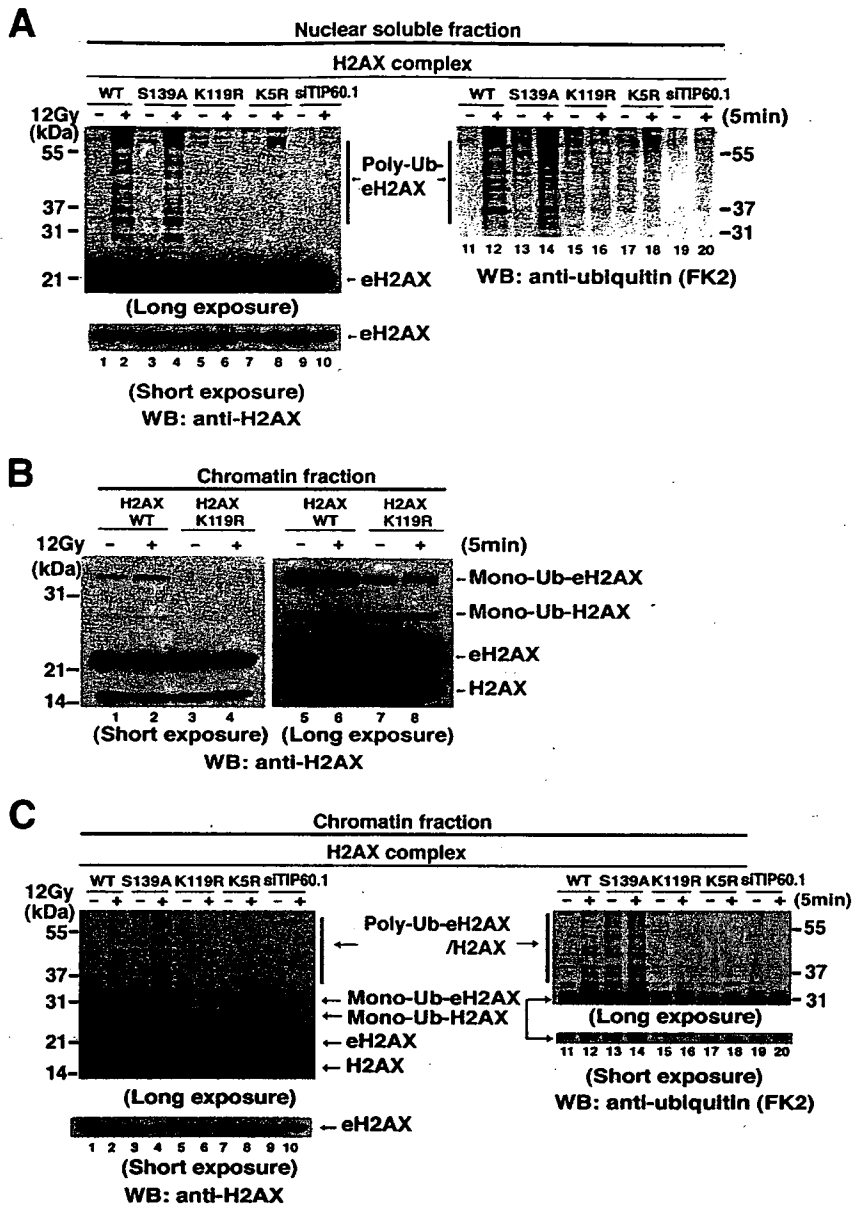


FIG. 2. Acetylation of H2AX regulated by TIP60 is required for the ubiquitination of H2AX upon DNA damage. (A and C) Wild-type eH2AX (lanes 1, 2, 11, and 12) and mutants eH2AX(S139A) (lanes 3, 4, 13, and 14), eH2AX(K119R) (lanes 5, 6, 15, and 16), and eH2AX(K5R) (lanes 7, 8, 17, and 18) were immunoaffinity purified from the nuclear soluble (A) and chromatin (C) fractions of cells stably expressing wild-type or mutant forms of eH2AX treated with IR (12 Gy) followed by a 5-min recovery. Wild-type eH2AX was also purified from TIP60 knockdown cells (siTIP60.1) expressing wild-type eH2AX (lanes 9, 10, 19, and 20). Proteins were analyzed by immunoblotting using anti-H2AX (left) and anti-ubiquitin (FK2) (right) antibodies. Asterisks indicate that the signals reacted with both anti-H2AX and anti-ubiquitin (FK2) antibodies. eH2AX was used as a loading control (bottom). (A) Unmodified eH2AX and polyubiquitinated eH2AX (poly-Ub-eH2AX) are indicated. (B) The monoubiquitination status of immunoaffinity-purified wild-type eH2AX (lanes 1, 2, 5, and 6) and the K119R mutant (lanes 3, 4, 7, and 8) from the chromatin fractions of cells treated with IR (12 Gy) followed by a 5-min recovery was analyzed by immunoblotting using anti-H2AX antibody. Unmodified eH2AX and mono-Ub-eH2AX were detected together with unmodified H2AX and mono-Ub-H2AX. (C) Poly-Ub-eH2AX and endogenous H2AX are indicated. WT, wild type; WB, Western blot.

matin fraction. Because the IR-induced acetylation was abolished by the eH2AX(K5R) mutation in the chromatin fraction (Fig. 3), we concluded that H2AX(K5) is the target of acetylation upon DSBs in the chromatin and nuclear soluble fractions. Importantly, DSB-induced mono- and polyubiquitination of eH2AX were significantly repressed by the eH2AX(K5R) mutation in the chromatin fraction as

in the nuclear soluble fraction of HeLa cells (Fig. 2C). The requirement for acetylation in the DSB-induced mono- and polyubiquitination of H2AX was confirmed by a coIP experiment using 293T cells expressing FLAG-tagged H2AX (K5R) and HA-tagged ubiquitin (see Fig. S3A in the supplemental material). Taken together, these findings suggest that TIP60 regulates the DSB-induced mono- and polyubi-

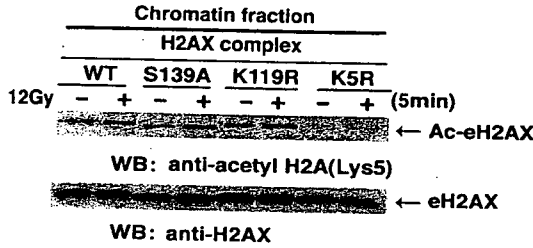


FIG. 3. H2AX is acetylated independent of phosphorylation and ubiquitination upon DNA damage. Wild-type and mutant eH2AX proteins (S139A, K119R, and K5R) were immunoaffinity purified from the chromatin fraction of HeLa cells treated with IR at 12 Gy followed by a 5-min recovery, and the acetylation status was analyzed by immunoblotting with the anti-acetyl-K5 of H2A (top). eH2AX was used as a loading control (bottom). Cells were treated with sodium butyrate (final concentration, 5 mM) for the detection of acetylation. WT, wild type; WB, Western blot.

uitination of H2AX in the chromatin fraction. If preexisting monoubiquitinated H2AX (mono-Ub-H2AX) in the chromatin fraction is the only source for DSB-induced polyubiquitination, the amount of mono-Ub-H2AX should be decreased. However, because the amount of mono-Ub-H2AX was increased upon DNA damage (Fig. 2C; also see Fig. S3A in the supplemental material), DNA damage can in-

duce the de novo polyubiquitination of H2AX in the chromatin fraction by TIP60.

To confirm the connection between acetylation and polyubiquitination, we examined the time courses of the H2AX modifications in the chromatin fraction of HeLa cells after IR. The polyubiquitination of eH2AX peaked sharply 2 to 5 min after IR and nearly paralleled its acetylation (Fig. 4A and B). The increase in mono-Ub-H2AX also peaked at 2 to 5 min (Fig. 4B). We also obtained comparable results in a coIP experiment using 293T cells expressing FLAG-tagged H2AX and HA-tagged ubiquitin (see Fig. S3B in the supplemental material). The similarities in the kinetics of acetylation and of the mono- and polyubiquitination of H2AX strongly suggest a preferential linkage of acetylation with de novo polyubiquitination of eH2AX in the chromatin fraction immediately after IR. Notably, the ratio of polyubiquitination to monoubiquitination of H2AX in the nuclear soluble fraction is much higher than that in the chromatin fraction. This suggests that the polyubiquitination but not the monoubiquitination of H2AX is involved in the release of H2AX from chromatin upon DNA damage. Collectively, these findings suggest that TIP60 facilitates H2AX release upon DNA damage via acetylation-dependent polyubiquitination of H2AX at the very early stage of DNA repair.

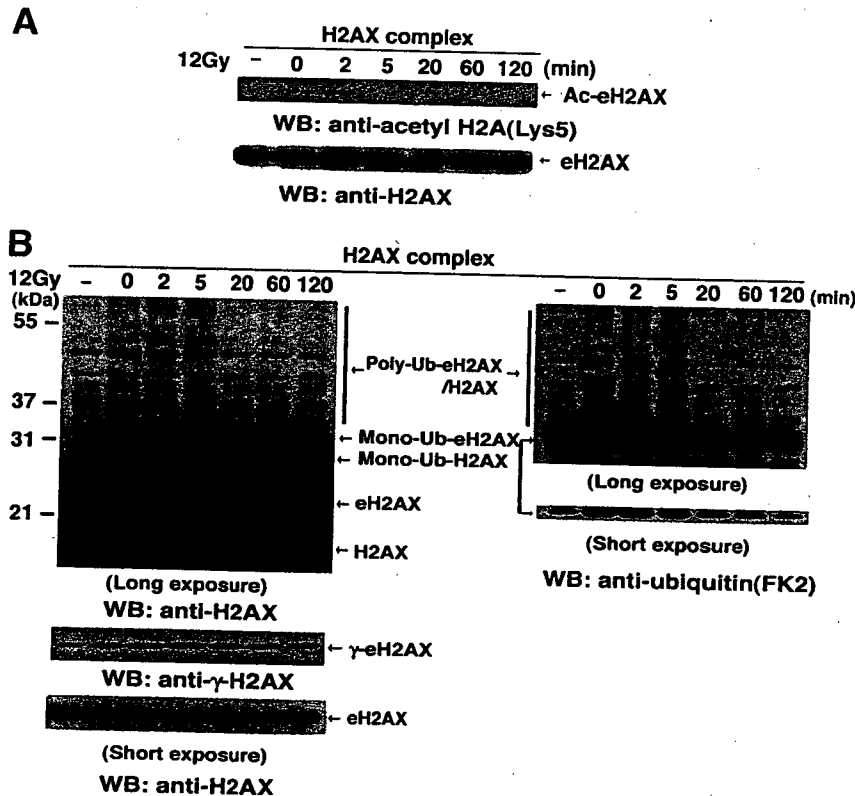


FIG. 4. Time course of acetylation, ubiquitination, and phosphorylation of H2AX after induction of DSBs. Wild-type eH2AX was immunoaffinity purified from the chromatin-bound fraction derived from HeLa cells stably expressing eH2AX at the indicated times of recovery after IR (12 Gy). (A) The acetylation status was analyzed by immunoblotting with the anti-acetyl-K5 of H2A (top). eH2AX was used as a loading control (bottom). Cells were treated with sodium butyrate (final concentration, 5 mM) for the detection of acetylation. (B) Proteins were analyzed by immunoblotting using anti-H2AX (top and bottom in left gel), anti- $\gamma$ -H2AX (middle in left gel), and antiubiquitin (FK2) (right) antibodies. eH2AX was used as a loading control (bottom in left gel). Asterisks indicate the bands reacted with both anti-H2AX and antiubiquitin (FK2) antibodies. WB, Western blot.

**Acetylation-dependent ubiquitination of H2AX upon DNA damage is independent of phosphorylation.** The above data provide evidence for the acetylation-dependent ubiquitination of H2AX upon DSBs by TIP60. However, the relationship between the DSB-induced acetylation-dependent ubiquitination and phosphorylation of H2AX remains unclear. To investigate this further, we examined the modification status of a phosphorylation mutant of H2AX [eH2AX(S139A)] after IR. Immunoblotting analysis using anti-H2AX and antiubiquitin (FK2) antibodies revealed that eH2AX(S139A) affinity purified from both the nuclear soluble and chromatin fractions were mono- and polyubiquitinated following IR (Fig. 2A and C). This finding was supported by a coIP experiment using 293T cells expressing FLAG-tagged H2AX(S139A) and HA-tagged ubiquitin (see Fig. S3A in the supplemental material). Moreover, eH2AX(S139A) in the chromatin fraction was acetylated after IR (Fig. 3). These findings suggest that phosphorylation is not required for either acetylation or ubiquitination after IR. Consistently, in contrast to what was seen for the acetylation and polyubiquitination of eH2AX, which peaked 2 to 5 min after IR, the level of phosphorylation was constant during the experiment (Fig. 4B). Taken together, these results indicated that acetylation-dependent ubiquitination is regulated independently of the phosphorylation of H2AX upon DNA damage.

To determine the biological consequences of the acetylation, ubiquitination, and phosphorylation of H2AX following DNA damage, we established HeLa cells expressing siRNAs targeted to the noncoding region of the endogenous H2AX for the reconstitution experiments with the expression of H2AX mutants (see Fig. S4A in the supplemental material). The expression of the GFP-H2AX wild type and GFP-H2AX mutants was not affected by the coexpression of H2AX siRNA (see Fig. S4A in the supplemental material). We found that following IR, the survival of HeLa cells expressing H2AX(K5R), H2AX(K119R), or H2AX(S139A) mutants was reduced compared to that seen for H2AX knockdown HeLa cells expressing wild-type eH2AX or for the parental HeLa cells ( $P < 0.01$ ) (see Fig. S4B in the supplemental material). These data suggest that along with H2AX phosphorylation, H2AX acetylation and ubiquitination play a significant role in cellular survival following DNA damage.

**The TIP60-UBC13 complex regulates the DSB-induced ubiquitination of H2AX.** In our previous study, we suggested that UBC13 can regulate the ubiquitination of H2AX after IR (64). Indeed, we found that UBC13 is included in eH2AX complexes that were affinity purified from either nuclear soluble or chromatin fractions and that the amount of UBC13 in the H2AX complexes was substantially increased following IR (Fig. 5A). We further analyzed the localization of GFP-tagged TIP60 or UBC13 expressed in GM02063 cells carrying DSBs along a microirradiated line. We found that both GFP-TIP60 and GFP-UBC13 accumulated at damaged sites 5 min after microirradiation (Fig. 5B). We confirmed that the integration of UBC13 into TIP60 purified from the nuclear soluble fraction is stimulated following IR (Fig. 5C). The ubiquitination of H2AX after the induction of DSBs was disturbed in the UBC13-depleted HeLa cells expressing UBC13 siRNA, confirming the direct dependence of the ubiquitination of H2AX on UBC13 in the DNA damage response (Fig. 5D; also see Fig.

S5 in the supplemental material). Collectively, these findings indicate that TIP60 interacts with UBC13 to facilitate the ubiquitination of H2AX in damaged chromatin.

**H2AX is released from damaged chromatin after induction of DSBs.** Following IR, the level of poly-Ub-H2AX appeared to increase more in the soluble nuclear fraction than in the chromatin-bound fraction (Fig. 2A and C). This indicated that a fraction of H2AX may undergo dynamic release from damaged chromatin. To examine the mobility of DSB-associated H2AX, we utilized a laser UVA microirradiation system to induce DSBs at the single-cell level (21, 51, 58). We first confirmed that H2AX is poly- and monoubiquitinated after the induction of DSBs by UV irradiation of bromodeoxyuridine-labeled cells (data not shown). We then performed photobleaching analysis to assess histone binding properties *in vivo* following the induction of DSBs with the laser UVA microirradiation system (20, 24, 27). We confirmed that the stably expressed GFP-H2AX proteins in HeLa and GM02063 cells share a range of physiological properties with the endogenous histone: GFP-H2AX was found to localize in chromatin throughout the cell cycle, similar to other histones, and the salt extraction profile was similar to that of the endogenous H2AX (data not shown) (44). We then performed iFRAP analysis (14, 37) of GFP-H2AX in combination with microirradiation to determine whether GFP-H2AX is released from damaged chromatin. In iFRAP experiments, immediately following microirradiation, all of the fluorescence (except in small regions of irradiated areas and in unirradiated areas) was bleached, and the remaining GFP-H2AX fluorescence was chased using LSM510 confocal microscopy. As a result, the remaining GFP-H2AX fluorescence within the irradiated area became significantly weaker than that in the unirradiated area (Fig. 6A and B), suggesting that GFP-H2AX can diffuse from chromatin only in the irradiated area. Thus, DNA damage provokes the release of GFP-H2AX from chromatin.

The dynamics of H2AX following DNA damage were examined by determining the fluorescence recovery of GFP-H2AX within two independent strips of a single nucleus, one in the irradiated area and the other in an unirradiated region, immediately following microirradiation (Fig. 6C). Rapid fluorescence recovery was observed in the irradiated region ( $27.6\% \pm 8.2\%$  at 260 s), whereas the fluorescence intensity in the unirradiated region did not change much during the observed time ( $5.0\% \pm 4.3\%$  at 260 s) ( $P < 0.000001$ ) (Fig. 6D; also see the video in the supplemental material). These findings also indicate that the fluorescence recovery in the irradiated region is due to the unbleached GFP-H2AX molecules released from damaged chromatin, because GFP-H2AX in the unirradiated area showed stable binding to chromatin (Fig. 6C and D). As a control, we observed that GFP-H2A in the irradiated area displays a recovery of fluorescence intensity slower ( $13.3\% \pm 8.4\%$  at 260 s) than that of GFP-H2AX ( $P < 0.0005$ ) (Fig. 6E).

Chromatin has been shown to move in response to DNA damage (4, 21). We quantified the dynamics of other core histones following DNA damage to determine whether this occurred. GFP-tagged H2B ( $18.3\% \pm 9.9\%$  at 260 s), H3 ( $11.4\% \pm 6.9\%$  at 260 s), and H4 ( $10.0\% \pm 4.3\%$  at 260 s) displayed slower recoveries of fluorescence than GFP-H2AX following the induction of DNA damage ( $P < 0.005$ ) (see Fig. S6 in the supplemental material). We noted that irradiation

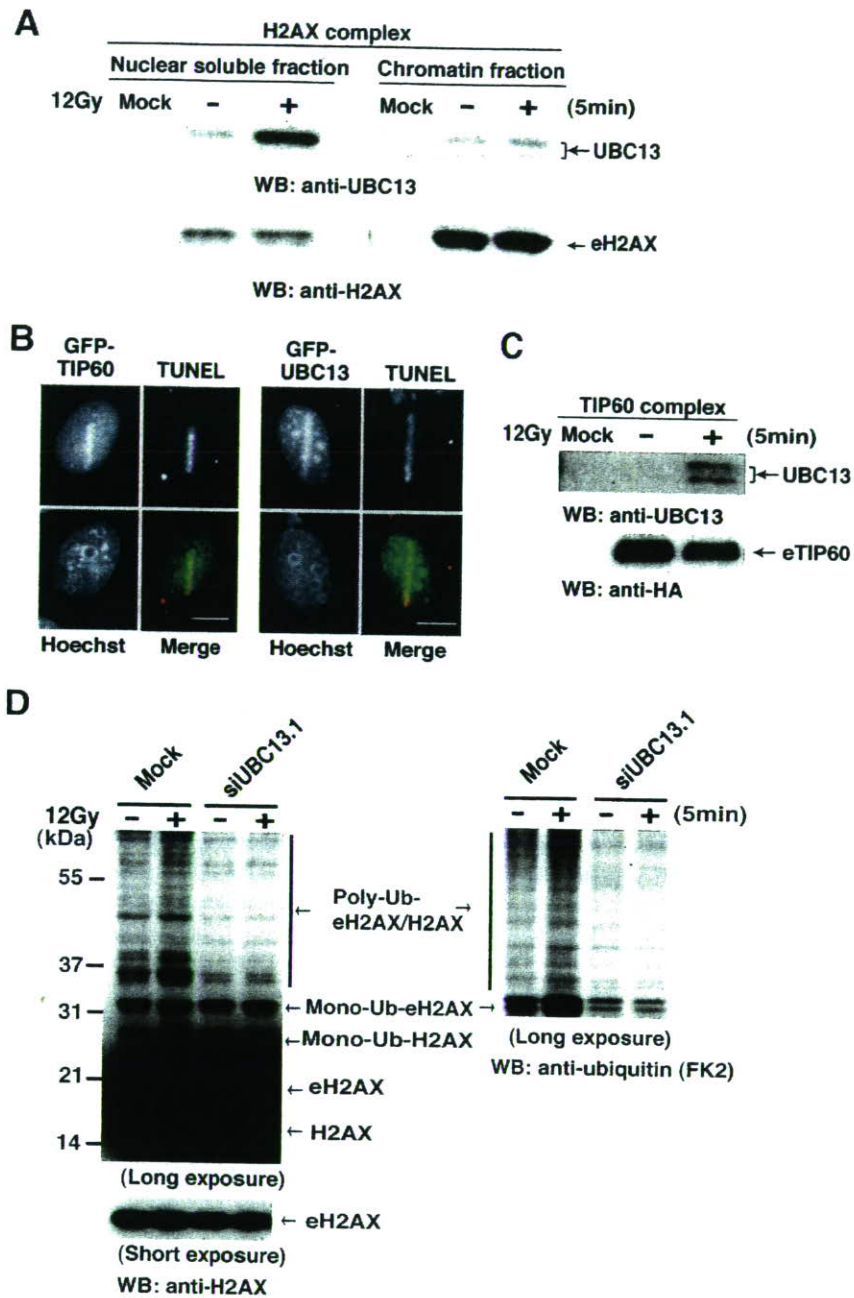


FIG. 5. UBC13, a ubiquitin-conjugating enzyme, interacts with TIP60 in damaged chromatin. (A) Affinity purification of eH2AX from the nuclear soluble (left) and chromatin (right) fractions of HeLa cells treated with IR at 12 Gy followed by a 5-min recovery. As a control, a mock purification was performed using nontransfected HeLa cells. UBC13 was detected by immunoblotting using anti-UBC13 antibody (top). eH2AX after a 5-min recovery from laser UVA microirradiation. TUNEL staining was performed to detect DSBs induced by microirradiation. GFP-TIP60/UBC13 and TUNEL signals are shown in green and red, respectively, in merged images. Scale bars, 10  $\mu$ m. (C) DSBs facilitate the interaction of UBC13 with the TIP60 complex. Immunoblot analysis of the mock control and the TIP60 complex affinity purified from the nuclear soluble fraction of cells treated with IR (12 Gy) followed by a 5-min recovery using anti-UBC13 antibody (top). eTIP60 was used as a loading control (bottom). (D) Wild-type eH2AX was affinity purified from the chromatin fraction of UBC13-specific siRNA (siUBC13.1)-expressing cells or the mock control cells treated with IR (12 Gy) followed by a 5-min recovery. Proteins were analyzed by immunoblotting using anti-H2AX (left) and antiubiquitin (FK2) (right) antibodies. WB, Western blot.

only subtly affected the recovery rate of the fluorescence intensity of H2B-GFP, which is the dimerization partner for all H2A variants, including H2AX. Because H2AX accounts for only 5 to 10% of the total H2A in chromatin, the DSB-induced release of H2AX may have a limited impact on the global

dynamics of total H2B. Fluorescence recovery rates reflect the amount of fluorescence molecules coming into the photo-bleached area. Therefore, the high fluorescence recovery rate of GFP-H2AX compared to those of other GFP-tagged core histones strongly suggests the release of GFP-H2AX molecules

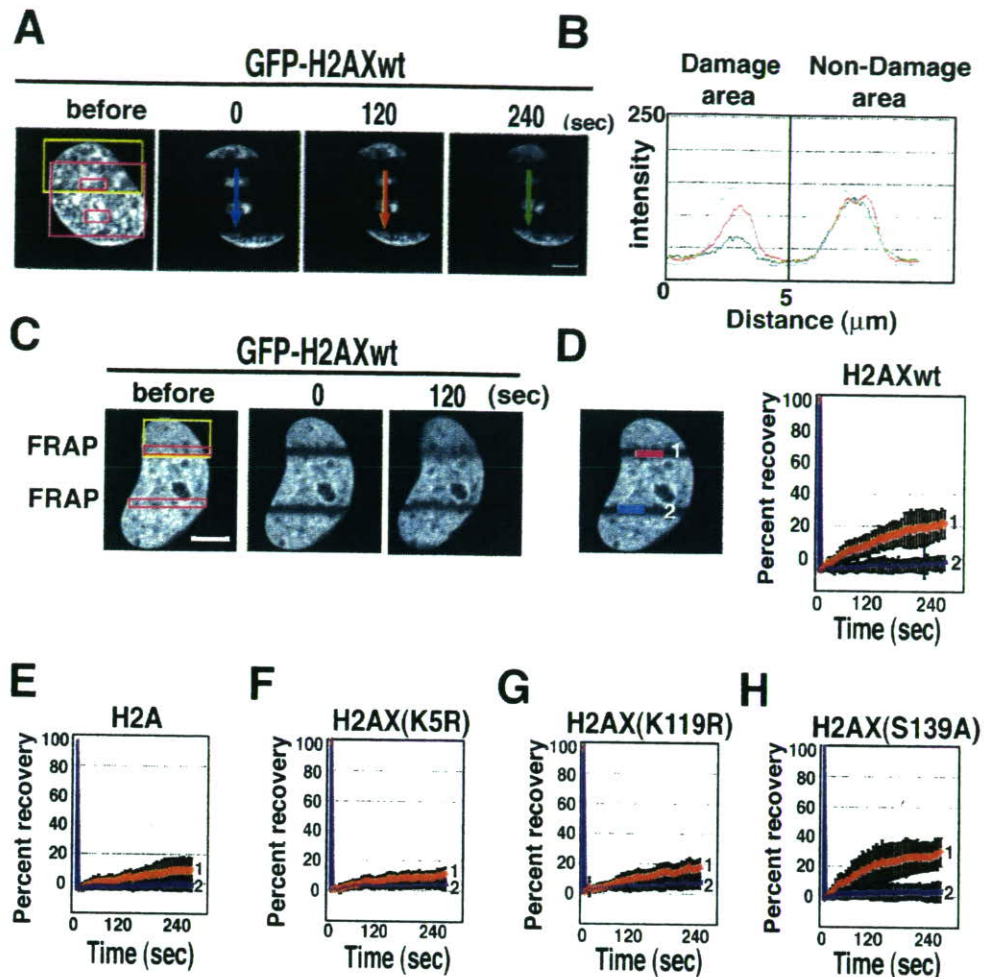


FIG. 6. In vivo dynamics of H2AX regulated by ubiquitination and acetylation of H2AX after induction of DSBs by microirradiation. (A) iFRAP analysis of GFP-H2AX in combination with microirradiation. Confocal images taken at indicated times after microirradiation are shown. DSBs were induced in GM02063 cells expressing GFP-H2AX by laser UVA microirradiation in the area indicated by a yellow box. Immediately after the induction of DSBs, fluorescence was bleached in the areas indicated by the red boxes with the 488-nm laser line of an Ar laser. Scale bar, 5  $\mu$ m. (B) Graph representation of fluorescence intensity versus distance along the arrows depicted in panel A. (C) FRAP analysis of GFP-H2AX after laser UVA microirradiation. GFP-H2AX was imaged before microirradiation, immediately after bleaching, and 120 s after bleaching (see the video in the supplemental material). Scale bar, 5  $\mu$ m. (D) Quantitative analysis of fluorescence recovery curves after bleaching of irradiated (1, red line) and control (2, blue line) areas. Values represent averages  $\pm$  standard errors for 14 cells. (E to H) Fluorescence recovery curves for GFP-H2A.1 ( $n = 11$ ) (E), GFP-H2AX(K5R) ( $n = 12$ ) (F), GFP-H2AX(K119R) ( $n = 10$ ) (G), and GFP-H2AX(S139A) ( $n = 15$ ) (H) in GM02063 cells over time in the microirradiated (red lines) and control (2, blue lines) regions.

from damaged chromatin into the microirradiated and photo-bleached area. Although we cannot exclude the possibility that a gross chromatin movement also contributed to the H2AX dynamics, such a gross movement alone is not sufficient to explain the observed H2AX dynamics. In support of this conclusion, the amount of  $\gamma$ -H2A(X) is lower near the DSBs than at distal sites in yeast (43). In fact, H2A(X) release upon DNA damage was also recently observed in yeast (S. Gasser, personal communication).

**H2AX release in the early response to DSBs is regulated by acetylation-dependent ubiquitination.** Following the establishment that H2AX is released from damaged chromatin upon DSBs, we next investigated the involvement of H2AX modifications in the DSB-induced release. Using FRAP, we examined the dynamics of GFP-tagged H2AX(K5R), H2AX(K119R), and H2AX(S139A) in GM02063 cells upon DSBs caused by micro-

irradiation. Compared to wild-type H2AX ( $27.6\% \pm 8.2\%$  at 260 s; Fig. 6D), both GFP-H2AX (K5R) ( $11.5\% \pm 4.4\%$  at 260 s; Fig. 6F) and GFP-H2AX(K119R) ( $17.5\% \pm 6.3\%$  at 260 s; Fig. 6G) showed reduced mobility following DNA damage ( $P < 0.005$ ). The fluorescence recovery of H2AX (S139A) ( $32.8\% \pm 8.5\%$  at 260 s) appeared comparable to that of wild-type H2AX (Fig. 6H). We also confirmed the reduced mobility of GFP-H2AX(K5R) and GFP-H2AX(K119R) after microirradiation in GM02063 cells by iFRAP analysis (data not shown). These results suggest a significant role of K5 acetylation and K119 ubiquitination in DSB-induced H2AX release. Conversely, the phosphorylation of H2AX(S139) does not appear to play a role in the release of H2AX following DNA damage.

**TIP60 and UBC13 regulate H2AX release following DNA damage.** To examine the role of TIP60 and UBC13, we per-

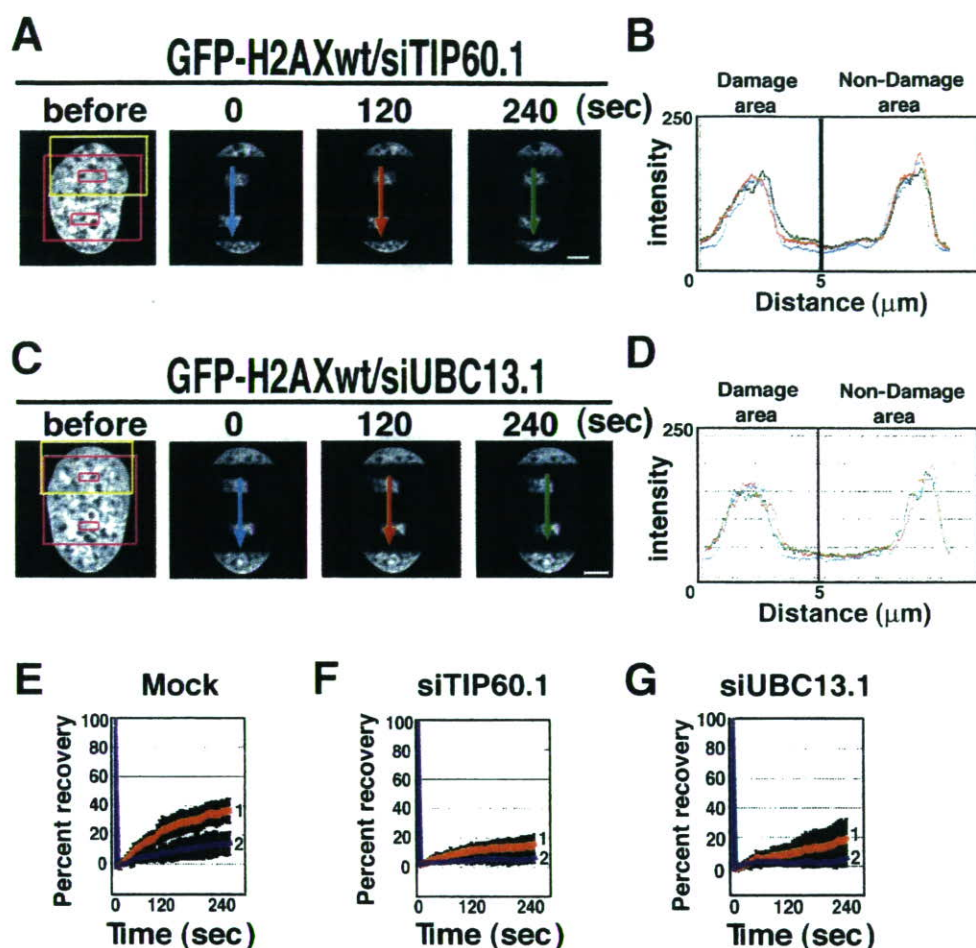


FIG. 7. TIP60 and UBC13 are required for the release of H2AX upon DNA damage. (A to D) iFRAP analysis of GFP-H2AX after microirradiation in GM02063 cells expressing TIP60 (siTIP60.1)- or UBC13 (siUBC13.1)-specific siRNAs was performed as described for Fig. 6A and B. Depletion of TIP60 or UBC13 suppressed the DSB-induced release of GFP-H2AX. Scale bars, 5  $\mu\text{m}$ . (E to G) Fluorescence recovery curves for GFP-H2AX in the microirradiated (red lines) and control (blue lines) regions in mock-transfected cells ( $n = 15$ ) (E) and for GFP-H2AX in GM02063 cells expressing TIP60-specific siRNA (siTIP60.1) ( $n = 10$ ) (F) or UBC13-specific siRNA (siUBC13.1) ( $n = 12$ ) (G).

formed iFRAP and FRAP analyses in TIP60 or UBC13 knock-down cells. Depletion of TIP60 by siRNA significantly reduced the diffusion of GFP-H2AX following microirradiation in iFRAP experiments (Fig. 7A and B). The involvement of TIP60 in the DSB-induced release of H2AX was confirmed by the reduced fluorescence recovery of GFP-H2AX in microirradiated regions of single nuclei in TIP60 knockdown cells ( $14.3\% \pm 7.7\%$  at 260 s;  $P < 0.001$ ; Fig. 7E and F; also see Fig. S2C in the supplemental material). Similar results were obtained in cells expressing a dominant-negative TIP60 HAT mutant (data not shown). UBC13 knockdown GM02063 cells also showed a significant reduction in GFP-H2AX mobility following microirradiation in iFRAP and FRAP experiments ( $20.1\% \pm 13.8\%$  at 260 s;  $P < 0.05$ ; Fig. 7C, D, and G). Taken together, these results are consistent with the conclusion that TIP60 and UBC13 control the damage-induced release of H2AX via the acetylation-ubiquitination pathway in the earlier stage of DNA repair.

The regulation of chromatin reorganization immediately after DNA damage by TIP60 in conjunction with UBC13 via the release of H2AX suggests the involvement of TIP60 in the subsequent DNA repair process. In support of this conclusion,

UBC13 is reported to be required for the recruitment/activation of the ubiquitin ligase function of BRCA1 and the subsequent formation of RAD51 nucleoprotein filaments at DSBs (64). To investigate the role of TIP60 in the DNA repair process, we examined RAD51 focus formation after IR in GM02063 cells expressing the TIP60 HAT mutant. RAD51 focus formation after IR was significantly disturbed in TIP60 HAT mutant-expressing cells (see Fig. S7 in the supplemental material). Although we cannot exclude the possibility that TIP60 regulates RAD51 focus formation independently of H2AX release in the early step of homologous recombination repair, it is possible that the TIP60-UBC13 complex is involved in the DNA repair process, especially homologous recombination repair, via H2AX release.

## DISCUSSION

In this study, we found that TIP60 HAT interacts with H2AX upon DNA damage and that H2AX is not only acetylated but also ubiquitinated just after the induction of DSBs in human cells. DSB-induced acetylation regulated by TIP60 is

required for the ubiquitination of H2AX. We identified the ubiquitin-conjugating enzyme UBC13 as a novel binding partner for TIP60 in the ubiquitination of H2AX following DSB formation. Interestingly, experiments using FRAP/iFRAP in conjunction with microirradiation indicated that the release of H2AX from damaged chromatin depends on the acetylation-ubiquitination pathway. Specifically, our findings indicate that the TIP60-UBC13 complex regulates the release via acetylation-dependent ubiquitination in the early stage of the DNA damage response.

We showed here that immediately after microirradiation, DSBs facilitate the interaction of TIP60 with UBC13 (Fig. 5B and C). Because TIP60-induced acetylation of H2AX is required for the polyubiquitination of H2AX upon DNA damage, the acetylation of H2AX may be involved in the recruitment of UBC13 to the damage site, or it may modulate the activity of UBC13 to facilitate the polyubiquitination of H2AX, leading to the release of H2AX. In our preliminary experiments, depletion of TIP60 by use of siRNA did not suppress the interaction of UBC13 with H2AX upon DNA damage (data not shown), suggesting that the acetylation of H2AX by TIP60 is not essential for the recruitment of UBC13 into the damage site. Therefore, the enzymatic activity of UBC13 may be induced by TIP60 through an unknown mechanism mediating H2AX polyubiquitination after the induction of DSBs.

At present, it is not clear how the polyubiquitination of H2AX regulates the release of H2AX. Because polyubiquitination by UBC13 often regulates protein function or protein-protein interactions (33), damage-induced polyubiquitination of H2AX by TIP60-UBC13 could be a signal for the recruitment of histone chaperone or chromatin-remodeling factors. The other possibility is that the structural change of H2AX by polyubiquitination might lead to the decreased affinity of H2AX for nucleosomes. Further studies are required to determine which of these possibilities is correct.

The DmTIP60-p400/Domino complex regulates the exchange of phospho-H2A.v with an unmodified H2A.v in vitro (22). Because p400 is included in the purified TIP60 complex and is required for UV-induced apoptosis in human cells (54), p400 may be involved in the release of H2AX in cooperation with the TIP60-UBC13 complex, leading to cell cycle progression or apoptosis. A previous study also showed that the TIP60-TRRAP complex is involved in homologous recombinational repair by acetylating histone H4 after the induction of DSBs (39). Although it remains unclear whether the TIP60-TRRAP complex participates in the release of H2AX, histone H4 acetylation by the TIP60-TRRAP complex may be needed to facilitate the polyubiquitination of H2AX by UBC13 during homologous recombinational repair. Therefore, to address the significance of the TIP60-UBC13 complex in H2AX release, it will be important to identify factors involved in this process within the TIP60 complex following the induction of DSBs.

A number of potential functions of H2AX in DNA damage response or DNA repair have been suggested.  $\gamma$ -H2AX has been proposed to function as a docking site for repair protein complexes to bind to broken DNA ends (5, 46).  $\gamma$ -H2AX may also keep the broken DNA ends tethered together with assembled repair factors to prevent aberrant repair of DSBs such as chromosomal translocations, because the loss of one H2AX allele results in a haploinsufficiency that compromises genomic

integrity and enhances genomic instability in the absence of p53 (5, 7). However, it is unclear whether the phosphorylation of H2AX is involved in the alteration of the chromatin structure to facilitate the access of repair proteins to the damaged chromatin. The release of H2AX via the acetylation-ubiquitination pathway immediately after the induction of DSBs may be involved in the opening of damaged chromatin for the access of repair proteins around DSBs. Thus, H2AX could play two distinct roles in the early steps of the DNA damage response: (i) phosphorylation by ATM or DNA protein kinase catalytic subunit to form  $\gamma$ -H2AX foci for the accumulation of repair factors and (ii) acetylation-dependent ubiquitination by TIP60-UBC13 to facilitate the release of H2AX for the alteration of chromatin structure at the damage site. Recently, RAP80 has been shown to bind ubiquitin polymers at DSBs for the recruitment of BRCA1 (17, 45, 59). Therefore, ubiquitinated H2AX could also provide a docking site for repair proteins such as  $\gamma$ -H2AX.

In addition to the direct role of TIP60 in chromatin reorganization, TIP60 plays other roles in cell cycle control and apoptosis by acetylating MYC or ATM (41, 47, 54). Recently, TIP60 was shown to acetylate p53 directly in the DNA damage response and to regulate the transcriptional regulation of the target genes of p53 (48, 50). Because DSBs facilitate the interaction of TIP60 with UBC13, p53 may also be polyubiquitinated by UBC13 during transcriptional regulation. It is also possible that some other signaling molecules could be acetylated and polyubiquitinated by TIP60-UBC13 upon the formation of DSBs. If so, acetylation-dependent polyubiquitination by TIP60-UBC13 in the DNA damage response may be required not only for the release of H2AX but also for transcriptional regulation in cell proliferation, cell cycle control, or apoptosis.

#### ACKNOWLEDGMENTS

We thank Y. Masuda, Y. Nakatani, J. Walter, T. Cremer, A. Yasui, T. Shiraki, and H. Kurumizaka for discussions and comments on the manuscript; S. Hatakeyama and K. I. Nakayama for providing the antibody to ubiquitin (FK2); P. Y. Perche for the GFP-H2A.1 construct; T. Kanda and G. Wahl for the H2B-GFP construct; H. Tagami for H2A-FLAG/HA-expressing HeLa cells; R. Waldren for editing the manuscript; and H. Suzuki for technical assistance.

This work was supported by the Hiroshima University 21st Century COE Program and grants-in-aid from the Ministry of Education, Culture, Sports, Science, and Technology of Japan.

#### REFERENCES

- Ahmad, K., and S. Henikoff. 2002. The histone variant H3.3 marks active chromatin by replication-independent nucleosome assembly. *Mol. Cell* 9:1191-1200.
- Andersen, P. L., H. Zhou, L. Pastushok, T. Moraes, S. McKenna, B. Ziola, M. J. Ellison, V. M. Dixit, and W. Xiao. 2005. Distinct regulation of Ubc13 functions by the two ubiquitin-conjugating enzyme variants Mms2 and Uev1A. *J. Cell Biol.* 170:745-755.
- Angelov, D., A. Molla, P. Y. Perche, F. Hans, J. Cote, S. Khochbin, P. Bourvet, and S. Dimitrov. 2003. The histone variant macroH2A interferes with transcription factor binding and SWI/SNF nucleosome remodeling. *Mol. Cell* 11:1033-1041.
- Aten, J. A., J. Stap, P. M. Krawczyk, C. H. van Oven, R. A. Hoebe, J. Essers, and R. Kanaar. 2004. Dynamics of DNA double-strand breaks revealed by clustering of damaged chromosome domains. *Science* 303:92-95.
- Bassing, C. H., and F. W. Alt. 2004. H2AX may function as an anchor to hold broken chromosomal DNA ends in close proximity. *Cell Cycle* 3:149-153.
- Bassing, C. H., K. F. Chua, J. Sekiguchi, H. Suh, S. R. Whittow, J. C. Fleming, B. C. Monroe, D. N. Ciccone, C. Yan, K. Vlasakova, D. M. Livingston, D. O. Ferguson, R. Scully, and F. W. Alt. 2002. Increased ionizing radiation sensitivity and genomic instability in the absence of histone H2AX. *Proc. Natl. Acad. Sci. USA* 99:8173-8178.

7. Bassing, C. H., H. Suh, D. O. Ferguson, K. F. Chua, J. Manis, M. Eckersdorff, M. Gleason, R. Bronson, C. Lee, and F. W. Alt. 2003. Histone H2AX: a dosage-dependent suppressor of oncogenic translocations and tumors. *Cell* 114:359-370.
8. Bergink, S., F. A. Salomons, D. Hoogstraten, T. A. Groothuis, H. de Waard, J. Wu, L. Yuan, E. Citterio, A. B. Houtsmuller, J. Neeffes, J. H. Hoetjmakers, W. Vermeulen, and N. P. Dantuma. 2006. DNA damage triggers nucleotide excision repair-dependent monoubiquitylation of histone H2A. *Genes Dev.* 20:1343-1352.
9. Bird, A. W., D. Y. Yu, M. G. Pray-Grant, Q. Qiu, K. E. Harmon, P. C. Megee, P. A. Grant, M. M. Smith, and M. F. Christman. 2002. Acetylation of histone H4 by Esa1 is required for DNA double-strand break repair. *Nature* 419:411-415.
10. Celeste, A., O. Fernandez-Capetillo, M. J. Kruhlak, D. R. Pilch, D. W. Staudt, A. Lee, R. F. Bonner, W. M. Bonner, and A. Nussenzweig. 2003. Histone H2AX phosphorylation is dispensable for the initial recognition of DNA breaks. *Nat. Cell Biol.* 5:675-679.
11. Downs, J. A., S. Allard, O. Jobin-Robitaille, A. Javaheri, A. Auger, N. Bouchard, S. J. Kron, S. P. Jackson, and J. Cote. 2004. Binding of chromatin-modifying activities to phosphorylated histone H2A at DNA damage sites. *Mol. Cell Biol.* 24:979-990.
12. Downs, J. A., M. C. Nussenzweig, and A. Nussenzweig. 2007. Chromatin dynamics and the preservation of genetic information. *Nature* 447:951-958.
13. Doyon, Y., W. Selleck, W. S. Lane, S. Tan, and J. Cote. 2004. Structural and functional conservation of the NuA4 histone acetyltransferase complex from yeast to humans. *Mol. Cell Biol.* 24:1884-1896.
14. Dunder, M., M. D. Hebert, T. S. Karpova, D. Stanek, H. Xu, K. B. Shpargel, U. T. Meier, K. M. Neugebauer, A. G. Matera, and T. Misteli. 2004. In vivo kinetics of Cajal body components. *J. Cell Biol.* 164:831-842.
15. Giannattasio, M., F. Lazzaro, P. Plevani, and M. Muzi-Falconi. 2005. The DNA damage checkpoint response requires histone H2B ubiquitination by Rad6-Brel and H3 methylation by Dot1. *J. Biol. Chem.* 280:9879-9886.
16. Ikura, T., V. V. Ogryzko, M. Grigoriev, R. Groisman, J. Wang, M. Horikoshi, R. Scully, J. Qin, and Y. Nakatani. 2000. Involvement of the TIP60 histone acetylase complex in DNA repair and apoptosis. *Cell* 102:463-473.
17. Kim, H., J. Chen, and X. Yu. 2007. Ubiquitin-binding protein RAP80 mediates BRCA1-dependent DNA damage response. *Science* 316:1202-1205.
18. Kimura, A., and M. Horikoshi. 1998. Tip60 acetylates six lysines of a specific class in core histones in vitro. *Genes Cells* 3:789-800.
19. Kimura, H. 2005. Histone dynamics in living cells revealed by photobleaching. *DNA Repair (Amsterdam)* 4:939-950.
20. Kimura, H., and P. R. Cook. 2001. Kinetics of core histones in living human cells: little exchange of H3 and H4 and some rapid exchange of H2B. *J. Cell Biol.* 153:1341-1353.
21. Kruhlak, M. J., A. Celeste, G. Dellaire, O. Fernandez-Capetillo, W. G. Muller, J. G. McNally, D. P. Bazett-Jones, and A. Nussenzweig. 2006. Changes in chromatin structure and mobility in living cells at sites of DNA double-strand breaks. *J. Cell Biol.* 172:823-834.
22. Kusch, T., L. Florens, W. H. Macdonald, S. K. Swanson, R. L. Glaser, J. R. Yates III, S. M. Abmayr, M. P. Washburn, and J. L. Workman. 2004. Acetylation by Tip60 is required for selective histone variant exchange at DNA lesions. *Science* 306:2084-2087.
23. Lou, Z., K. Minter-Dykhouse, S. Franco, M. Gostissa, M. A. Rivera, A. Celeste, J. P. Manis, J. van Deursen, A. Nussenzweig, T. T. Paull, F. W. Alt, and J. Chen. 2006. MDC1 maintains genomic stability by participating in the amplification of ATM-dependent DNA damage signals. *Mol. Cell* 21:187-200.
24. Louters, L., and R. Chalkley. 1985. Exchange of histones H1, H2A, and H2B in vivo. *Biochemistry* 24:3080-3085.
25. Masumoto, H., D. Hawke, R. Kobayashi, and A. Verreault. 2005. A role for cell-cycle-regulated histone H3 lysine 56 acetylation in the DNA damage response. *Nature* 436:294-298.
26. Meneghini, M. D., M. Wu, and H. D. Madhani. 2003. Conserved histone variant H2A.Z protects euchromatin from the ectopic spread of silent heterochromatin. *Cell* 112:725-736.
27. Misteli, T., A. Gunjan, R. Hock, M. Bustin, and D. T. Brown. 2000. Dynamic binding of histone H1 to chromatin in living cells. *Nature* 408:877-881.
28. Mizuguchi, G., X. Shen, J. Landry, W. H. Wu, S. Sen, and C. Wu. 2004. ATP-driven exchange of histone H2AZ variant catalyzed by SWR1 chromatin remodeling complex. *Science* 303:343-348.
29. Morrison, A. J., J. Highland, N. J. Krogan, A. Arbel-Eden, J. F. Greenblatt, J. E. Haber, and X. Shen. 2004. INO80 and gamma-H2AX interaction links ATP-dependent chromatin remodeling to DNA damage repair. *Cell* 119:767-775.
30. Murr, R., J. I. Loizou, Y. G. Yang, C. Cuenin, H. Li, Z. Q. Wang, and Z. Herceg. 2006. Histone acetylation by Trapp-Tip60 modulates loading of repair proteins and repair of DNA double-strand breaks. *Nat. Cell Biol.* 8:91-99.
31. Nakatani, Y., and V. Ogryzko. 2003. Immunoaffinity purification of mammalian protein complexes. *Methods Enzymol.* 370:430-444.
32. Petrini, J. H., and T. H. Stracker. 2003. The cellular response to DNA double-strand breaks: defining the sensors and mediators. *Trends Cell Biol.* 13:458-462.
33. Pickart, C. M. 2001. Ubiquitin enters the new millennium. *Mol. Cell* 8:499-504.
34. Polanowska, J., J. S. Martin, T. Garcia-Muse, M. I. Petalcorin, and S. J. Boulton. 2006. A conserved pathway to activate BRCA1-dependent ubiquitylation at DNA damage sites. *EMBO J.* 25:2178-2188.
35. Polo, S. E., and G. Almouzni. 2006. Chromatin assembly: a basic recipe with various flavours. *Curr. Opin. Genet. Dev.* 16:104-111.
36. Polo, S. E., D. Roche, and G. Almouzni. 2006. New histone incorporation marks sites of UV repair in human cells. *Cell* 127:481-493.
37. Rabut, G., V. Doye, and J. Ellenberg. 2004. Mapping the dynamic organization of the nuclear pore complex inside single living cells. *Nat. Cell Biol.* 6:1114-1121.
38. Redon, C., D. Pilch, E. Rogakou, O. Sedelnikova, K. Newrock, and W. Bonner. 2002. Histone H2A variants H2AX and H2AZ. *Curr. Opin. Genet. Dev.* 12:162-169.
39. Robert, F., S. Hardy, Z. Nagy, C. Baldeyron, R. Murr, U. Dery, J. Y. Masson, D. Papadopoulos, Z. Herceg, and L. Tora. 2006. The transcriptional histone acetyltransferase cofactor TRRAP associates with the MRN repair complex and plays a role in DNA double-strand break repair. *Mol. Cell Biol.* 26:402-412.
40. Rogakou, E. P., D. R. Pilch, A. H. Orr, V. S. Ivanova, and W. M. Bonner. 1998. DNA double-stranded breaks induce histone H2AX phosphorylation on serine 139. *J. Biol. Chem.* 273:5858-5868.
41. Sapountzi, V., I. R. Logan, and C. N. Robson. 2006. Cellular functions of TIP60. *Int. J. Biochem. Cell Biol.* 38:1496-1509.
42. Schwartz, B. E., and K. Ahmad. 2005. Transcriptional activation triggers deposition and removal of the histone variant H3.3. *Genes Dev.* 19:804-814.
43. Shroff, R., A. Arbel-Eden, D. Pilch, G. Ira, W. M. Bonner, J. H. Petrini, J. E. Haber, and M. Lichten. 2004. Distribution and dynamics of chromatin modification induced by a defined DNA double-strand break. *Curr. Biol.* 14:1703-1711.
44. Siino, J. S., I. B. Nazarov, M. P. Svetlova, L. V. Solovjeva, R. H. Adamson, I. A. Zelenkaya, P. M. Yau, E. M. Bradbury, and N. V. Tomilin. 2002. Photobleaching of GFP-labeled H2AX in chromatin: H2AX has low diffusional mobility in the nucleus. *Biochem. Biophys. Res. Commun.* 297:1318-1323.
45. Sobhian, B., G. Shao, D. R. Lilli, A. C. Cultane, L. A. Moreau, B. Xia, D. M. Livingston, and R. A. Greenberg. 2007. RAP80 targets BRCA1 to specific ubiquitin structures at DNA damage sites. *Science* 316:1198-1202.
46. Stucki, M., and S. P. Jackson. 2006. gammaH2AX and MDC1: anchoring the DNA-damage-response machinery to broken chromosomes. *DNA Repair (Amsterdam)* 5:534-543.
47. Sun, Y., X. Jiang, S. Chen, N. Fernandes, and B. D. Price. 2005. A role for the Tip60 histone acetyltransferase in the acetylation and activation of ATM. *Proc. Natl. Acad. Sci. USA* 102:13182-13187.
48. Sykes, S. M., H. S. Mellert, M. A. Holbert, K. Li, R. Marmorstein, W. S. Lane, and S. B. McMahon. 2006. Acetylation of the p53 DNA-binding domain regulates apoptosis induction. *Mol. Cell* 24:841-851.
49. Tagami, H., D. Ray-Gallet, G. Almouzni, and Y. Nakatani. 2004. Histone H3.1 and H3.3 complexes mediate nucleosome assembly pathways dependent or independent of DNA synthesis. *Cell* 116:51-61.
50. Tang, Y., J. Luo, W. Zhang, and W. Gu. 2006. Tip60-dependent acetylation of p53 modulates the decision between cell-cycle arrest and apoptosis. *Mol. Cell* 24:827-839.
51. Tashiro, S., J. Walter, A. Shinohara, N. Kamada, and T. Cremer. 2000. Rad51 accumulation at sites of DNA damage and in postreplicative chromatin. *J. Cell Biol.* 150:283-291.
52. Thiriet, C., and J. J. Hayes. 2005. Chromatin in need of a fix: phosphorylation of H2AX connects chromatin to DNA repair. *Mol. Cell* 18:617-622.
53. Tsukuda, T., A. B. Fleming, J. A. Nickoloff, and M. A. Osley. 2005. Chromatin remodelling at a DNA double-strand break site in *Saccharomyces cerevisiae*. *Nature* 438:379-383.
54. Tyceta, S., M. Vandromme, G. Legube, M. Chevillard-Briet, and D. Trouche. 2006. Tip60 and p400 are both required for UV-induced apoptosis but play antagonistic roles in cell cycle progression. *EMBO J.* 25:1680-1689.
55. Utley, R. T., N. Lacoste, O. Jobin-Robitaille, S. Allard, and J. Cote. 2005. Regulation of NuA4 histone acetyltransferase activity in transcription and DNA repair by phosphorylation of histone H4. *Mol. Cell Biol.* 25:8179-8190.
56. van Attikum, H., O. Fritsch, B. Hohn, and S. M. Gasser. 2004. Recruitment of the INO80 complex by H2A phosphorylation links ATP-dependent chromatin remodeling with DNA double-strand break repair. *Cell* 119:777-788.
57. van Attikum, H., and S. M. Gasser. 2005. The histone code at DNA breaks: a guide to repair? *Nat. Rev. Mol. Cell Biol.* 6:757-765.
58. Walter, J., T. Cremer, K. Miyagawa, and S. Tashiro. 2003. A new system for laser-UVA-microirradiation of living cells. *J. Microsc.* 209:71-75.
59. Wang, B., S. Matsuoka, B. A. Ballif, D. Zhang, A. Smogorzewska, S. P. Gygi,

- and S. J. Elledge. 2007. Abraxas and RAP80 form a BRCA1 protein complex required for the DNA damage response. *Science* 316:1194–1198.
60. Wang, H., L. Zhai, J. Xu, H. Y. Joo, S. Jackson, H. Erdjument-Bromage, P. Tempst, Y. Xiong, and Y. Zhang. 2006. Histone H3 and H4 ubiquitylation by the CUL4-DDB-ROC1 ubiquitin ligase facilitates cellular response to DNA damage. *Mol. Cell* 22:383–394.
61. West, M. H., and W. M. Bonner. 1980. Histone 2A, a heteromorphous family of eight protein species. *Biochemistry* 19:3238–3245.
62. Wu, W. H., S. Alami, E. Luk, C. H. Wu, S. Sen, G. Mizuguchi, D. Wei, and C. Wu. 2005. Swc2 is a widely conserved H2AZ-binding module essential for ATP-dependent histone exchange. *Nat. Struct. Mol. Biol.* 12:1064–1071.
63. Xie, A., N. Puget, I. Shim, S. Odate, I. Jarzyna, C. H. Bassing, F. W. Alt, and R. Scully. 2004. Control of sister chromatid recombination by histone H2AX. *Mol. Cell* 16:1017–1025.
64. Zhao, G. Y., E. Sonoda, L. J. Barber, H. Oka, Y. Murakawa, K. Yamada, T. Ikura, X. Wang, M. Kobayashi, K. Yamamoto, S. J. Boulton, and S. Takeda. 2007. A critical role for the ubiquitin-conjugating enzyme Ubc13 in initiating homologous recombination. *Mol. Cell* 25:663–675.

# Dynamics of human replication factors in the elongation phase of DNA replication

Yuji Masuda<sup>1,\*</sup>, Miki Suzuki<sup>1</sup>, Jinlian Piao<sup>1</sup>, Yongqing Gu<sup>1</sup>, Toshiki Tsurimoto<sup>2</sup> and Kenji Kamiya<sup>1</sup>

<sup>1</sup>Research Institute for Radiation Biology and Medicine, Hiroshima University, Hiroshima 734-8553, Japan and <sup>2</sup>Department of Biology, School of Sciences, Kyushu University, Fukuoka 812-8581, Japan

Received July 19, 2007; Revised September 17, 2007; Accepted September 19, 2007

## ABSTRACT

In eukaryotic cells, DNA replication is carried out by coordinated actions of many proteins, including DNA polymerase  $\delta$  (pol  $\delta$ ), replication factor C (RFC), proliferating cell nuclear antigen (PCNA) and replication protein A. Here we describe dynamic properties of these proteins in the elongation step on a single-stranded M13 template, providing evidence that pol  $\delta$  has a distributive nature over the 7 kb of the M13 template, repeating a frequent dissociation–association cycle at growing 3′-hydroxyl ends. Some PCNA could remain at the primer terminus during this cycle, while the remainder slides out of the primer terminus or is unloaded once pol  $\delta$  has dissociated. RFC remains around the primer terminus through the elongation phase, and could probably hold PCNA from which pol  $\delta$  has detached, or reload PCNA from solution to restart DNA synthesis. Furthermore, we suggest that a subunit of pol  $\delta$ , POLD3, plays a crucial role in the efficient recycling of PCNA during dissociation–association cycles of pol  $\delta$ . Based on these observations, we propose a model for dynamic processes in elongation complexes.

## INTRODUCTION

In eukaryotic cells, DNA replication is carried out by coordinated actions of many proteins. It has been demonstrated that the elongation process can be reconstituted with distinct protein factors, DNA polymerase  $\delta$  (pol  $\delta$ ), replication factor C (RFC), proliferating cell nuclear antigen (PCNA) and replication protein A (RPA) (1–3). These replication factors, in addition to the polymerase  $\alpha$ -primase complex (pol  $\alpha$ ), are required components of the *in vitro* simian virus 40 (SV40) replication system (4). The pol  $\delta$  heterotetrameric complex, consisting of 125, 66, 50 and 12 kDa proteins (5),

is the major polymerase involved in chromosomal replication in eukaryotic cells. RFC is composed of one large subunit (145 kDa) and four smaller ones (40, 38, 37 and 36 kDa) (6,7) and has DNA-dependent ATPase activity, loading sliding clamp PCNA onto DNA (6,8). PCNA itself is a homotrimeric ring-shaped protein with a molecular mass of 29 kDa for each monomer, which encircles double-stranded DNA (9,10). The likely role of PCNA in pol  $\delta$  replication is in stabilizing the pol  $\delta$ –DNA interaction to maintain the processivity of the polymerase (11–17). RPA is a heterotrimeric single-stranded (ss) DNA-binding protein, consisting of 70, 32 and 14 kDa proteins, required for the initiation and elongation phases of DNA replication (18).

The initiation phase of DNA replication with these protein factors has been investigated intensively, and it has been demonstrated that their actions are well coordinated (19–26). An important process is the switch from pol  $\alpha$  to pol  $\delta$  (24), mediated by RFC (20,22,24,26).

After an elongation complex is once established, concerted actions of these protein components could still be required. However, the architecture and actions within elongation complexes remain obscure. It is generally believed that an elongation complex containing pol  $\delta$  and PCNA, but not RFC, is somehow extremely stable (27). However, we have obtained surprising results, revealing a markedly dynamic picture for elongation complexes consisting of pol  $\delta$ , PCNA and RFC. We thus have evidence that pol  $\delta$  frequently repeats a dissociation–association cycle at growing 3′-hydroxyl ends. RFC appears to remain at the primer terminus throughout the elongation phase, probably holding PCNA from which pol  $\delta$  has detached, with the potential to catalyze unloading of PCNA. Once pol  $\delta$  dissociates from a growing 3′-hydroxyl end, a significant fraction of PCNA may remain at the primer terminus through interaction with RFC, while the remainder may be unloaded by RFC or slide out of the primer terminus. RFC persisting around primer termini then may reload PCNA from solution to restart DNA synthesis. In addition, characterization of the dynamic properties

\*To whom correspondence should be addressed. Tel: +81 82 257 5893; Fax: +81 82 257 5843; Email: masudayu@hiroshima-u.ac.jp

of the same protein factors with a subassembly of pol  $\delta$  lacking the POLD3 subunit revealed a crucial function of POLD3 in the efficient recycling of PCNA.

## MATERIALS AND METHODS

### Plasmids

The expression plasmid for human PCNA was as described earlier (28) and that for human RPA, p11d-tRPA (29), was a generous gift of Dr Marc S. Wold (University of Iowa College of Medicine, Iowa City, Iowa). Human cDNAs for pol  $\delta$  and RFC were amplified from a HeLa cDNA library introducing a cutting site of NdeI at the start codon. The expression plasmids are listed in Supplementary Table 1, and details for their construction are described in the Supplementary Data.

### Proteins

All proteins used in this study were overproduced in *Escherichia coli* cells (Supplementary Table 1) and purified by conventional column chromatography. During all purification steps, induced proteins were monitored by SDS-PAGE followed by staining with Coomassie Brilliant Blue R-250 (CBB) or western blotting. Protein concentrations were determined by Bio-Rad protein assay using BSA (Bio-Rad) as the standard. The procedures are described in the Supplementary Data.

### Pol $\delta$ holoenzyme assays on single-stranded (ss) mp18 DNA

DNA polymerase activity was measured with reference to incorporation of [ $\alpha$ - $^{32}$ P]dTMP. The standard reaction mixture (25  $\mu$ l) contained 20 mM HEPES-NaOH (pH 7.5), 50 mM NaCl, 0.2 mg/ml BSA, 1 mM DTT, 10 mM MgCl<sub>2</sub>, 1 mM ATP, 0.1 mM each of dGTP, dATP, dCTP and [ $\alpha$ - $^{32}$ P]dTTP, 33 fmol (240 pmol for nucleotides) of singly primed ss mp18 DNA (the 36-mer primer, CAGGGTTTTCCCAGTCACGACGTTGTAAACGACGG is complementary to 6330–6295 nt) (30), 1.0  $\mu$ g (9.1 pmol) of RPA, 86 ng (1.0 pmol as a trimer) of PCNA, 75 ng (260 fmol) of RFC and 90 ng (380 fmol) of pol  $\delta$ . In the reactions with HincII, 10 U of the enzyme (Takara Bio Inc.) were introduced into the standard reaction mixture. Reaction mixtures lacking pol  $\delta$  were pre-incubated at 30°C for 1 min, then reactions were started by addition of pol  $\delta$ . After incubation at 30°C for 10 min, reactions were terminated with 2  $\mu$ l of 300 mM EDTA, and the mixtures were immediately chilled on ice. Five-microliter samples were spotted on DE81 paper (Whatman), which was washed three times with 0.5 M Na<sub>2</sub>HPO<sub>4</sub>. The amount of incorporated [ $\alpha$ - $^{32}$ P]dTMP was determined as the radioactivity retained on the paper (31). For electrophoretic analysis of replication products, 5  $\mu$ l samples were mixed with 1  $\mu$ l of loading buffer (150 mM NaOH/10 mM EDTA/6% sucrose/0.1% bromophenol blue), and electrophoresed on 0.7% alkaline-agarose gels as described (32). To detect the products by Southern blotting, the newly synthesized strands were hybridized with a 5'- $^{32}$ P-labeled oligonucleotide (GCACCCAGGCTTTACACTTTATGCTTCCGGCTCGTATGTTGTG

TGGAATTGTGAGCGGATAACAATTCACACAGGAAACAGCTATGACCATGATTAC). For linearization of ss mp18 DNA before reactions, an oligonucleotide, CAGGGTTTTCCCAGTCACGACGTTGTAAACGACGGCCAGTGCCAAGCTTGCATGCCTGCAGGTCGACTCTAGAGGATCCCCGGGTACCGAGCTCGAATT, was annealed to the template.

### Isolation of PCNA on DNA bound to magnetic beads

The 5'-biotinylated primer (CTCTCTCTCTCTCTCTCTCAGGGTTTTCCCAGTCACGACGTTGTAAACGACGG) was annealed to 33 fmol ss mp18 DNA, immobilized onto a 15- $\mu$ l suspension of streptavidin magnetic beads, M280 (Dynabeads) in 20 mM HEPES-NaOH (pH 7.5), 50 mM NaCl, 0.2 mg/ml BSA, 1 mM DTT by incubation at room temperature for 30 min and chilled on ice. The buffer condition of the mixture was adjusted to that of the pol  $\delta$  standard assay. For the reaction with HincII, 10 U of the enzyme (Takara Bio Inc.) were introduced into the standard reaction mixture. Reaction mixtures lacking pol  $\delta$  were pre-incubated at 30°C for 1 min, then pol  $\delta$  or buffer (as control) was introduced into the reaction mixture. After incubation at 30°C for 10 min, reactions were terminated with 2  $\mu$ l of 300 mM EDTA, and then the mixtures were immediately chilled on ice. Subsequent washes were carried out at 4°C using a Dynal magnet with 40  $\mu$ l of wash buffer [20 mM HEPES-NaOH (pH 7.5), 0.5 M NaCl, 0.2 mg/ml BSA, 1 mM DTT, 1 mM EDTA] four times. The beads were boiled in sample loading buffer and proteins were separated on a SDS 4–20% gradient polyacrylamide gel, blotted onto a nitrocellulose membrane, and probed with an anti-PCNA antibody (Santa Cruz, sc-7907). Detection was achieved with an ECL chemiluminescence kit (GE Healthcare Life Science). Different exposures of the blot were photographed with a CCD camera and quantified.

## RESULTS

### Reconstitution of DNA synthesis

We initially tried to establish procedures to purify the replication proteins (pol  $\delta$ , RFC, PCNA and RPA), at quantities sufficient for detailed biochemical studies. Because it has been shown that bacterial systems are very powerful for large-scale production of PCNA and RPA as complexes (24,28,29), we developed expression systems for heterotetrameric pol  $\delta$  and heteropentameric RFC in *E. coli* and the complexes were then purified by conventional column chromatography (Figure 1A).

First, we measured activities of purified proteins on singly primed ss mp18 DNA. In this assay, all of the protein components, RPA, PCNA and RFC, were found to be required for maximum activity of pol  $\delta$  (Figure 1B) (6,33,34). In the reaction for 10 min, we detected a long product, probably corresponding to the full-size mp18 DNA (7.2 kb) (Figure 1B), and the amount increased with further incubation (Figure 1C). The size of the products was heterogeneous, indicating several pausing sites. Omitting PCNA or RFC from the reaction mixture

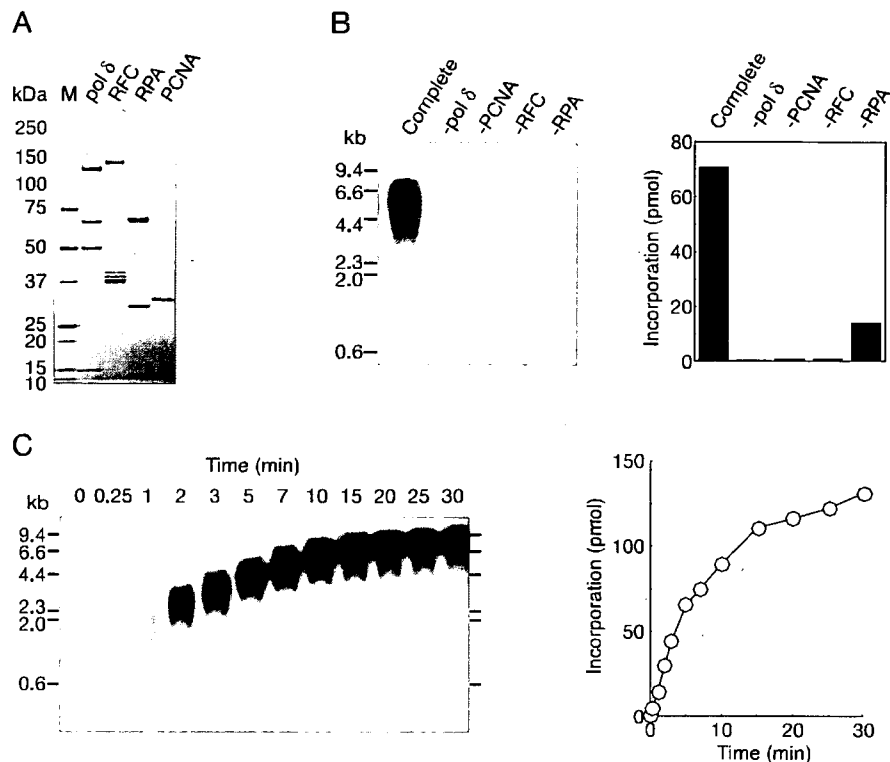


**Figure 1.** Reconstitution of DNA replication with recombinant replication factors on singly primed ss mp18 DNA. (A) SDS-PAGE analysis of purified recombinant proteins. Pol  $\delta$  (2.4  $\mu$ g), RFC (1.5  $\mu$ g), RPA (1.2  $\mu$ g) and PCNA (0.8  $\mu$ g) were loaded on a SDS 4–20% gradient polyacrylamide gel and stained with CBB. (B) Requirement of replication factors for synthesis of singly primed ss mp18 DNA. Reactions were carried out for 10 min under the conditions described in the Materials and Methods section or omitting one replication factor. Products were analyzed by 0.7% alkaline-agarose gel electrophoresis as described in the Materials and Methods section. Incorporation of dNMP was measured as described in the Materials and Methods section. (C) Time course of the reaction of DNA synthesis. The reaction products were analyzed by the same procedures as for (B).

resulted in virtually no incorporation of dNMP (Figure 1B). In the absence of RPA, heterogeneity in the length of the products was emphasized (Figure 1B) (6,34,35). Under the experimental conditions used, efficient dNMP incorporation was observed within the first 5 min, and then DNA synthesis continued at slower rates (Figure 1C). These results indicated that the recombinant proteins efficiently interacted with each other in the holoenzyme assay.

#### Differential modes of action of protein components on mp18 replication

Theoretically, proteins act during replication in two distinct modes (32). Some proteins remain associated continuously with the growing 3'-hydroxyl end (acting processively), and others repeat a cycle of association and dissociation (acting distributively). The distributive factors have to be reloaded many times from solution during elongation, while the processive factors are loaded only once at the initiation.

How each of the proteins acts during replication on ss mp18 DNA can be investigated (32) as described below. If a protein acts distributively, then the product size is expected to vary proportionally with the concentration of the protein in the reaction mixture; the average size

of products should be shorter at lower concentrations of the proteins because association of the protein to primer termini would be random and all primer termini would be utilized with the same efficiency (Figure 2A). On the other hand, if a protein acts processively, limiting its concentration in solution would be expected to affect only the frequency of the first assembly event (initiation), but not the size of products (Figure 2B). If the association and dissociation rates were much faster than other chemical steps, the binding process would not be rate limiting, and the incorporation rate of dNMP would not vary (Figure 2A and B, right panels). In the following experiments, we investigated the mode of action of proteins by analyzing size distributions of products by electrophoresis on agarose gels under denaturing conditions.

First, the concentration of pol  $\delta$  was varied in the presence of saturating amounts of the auxiliary proteins, and the product size was analyzed by alkaline-agarose gel electrophoresis (Figure 2C). The results showed that the amount and length of the products increased as more pol  $\delta$  was added to the reaction mixture (Figure 2C), implying that pol  $\delta$  frequently dissociated from the growing 3'-hydroxyl end and reassociated randomly with free 3'-hydroxyl ends (34–36). The dissociation might be

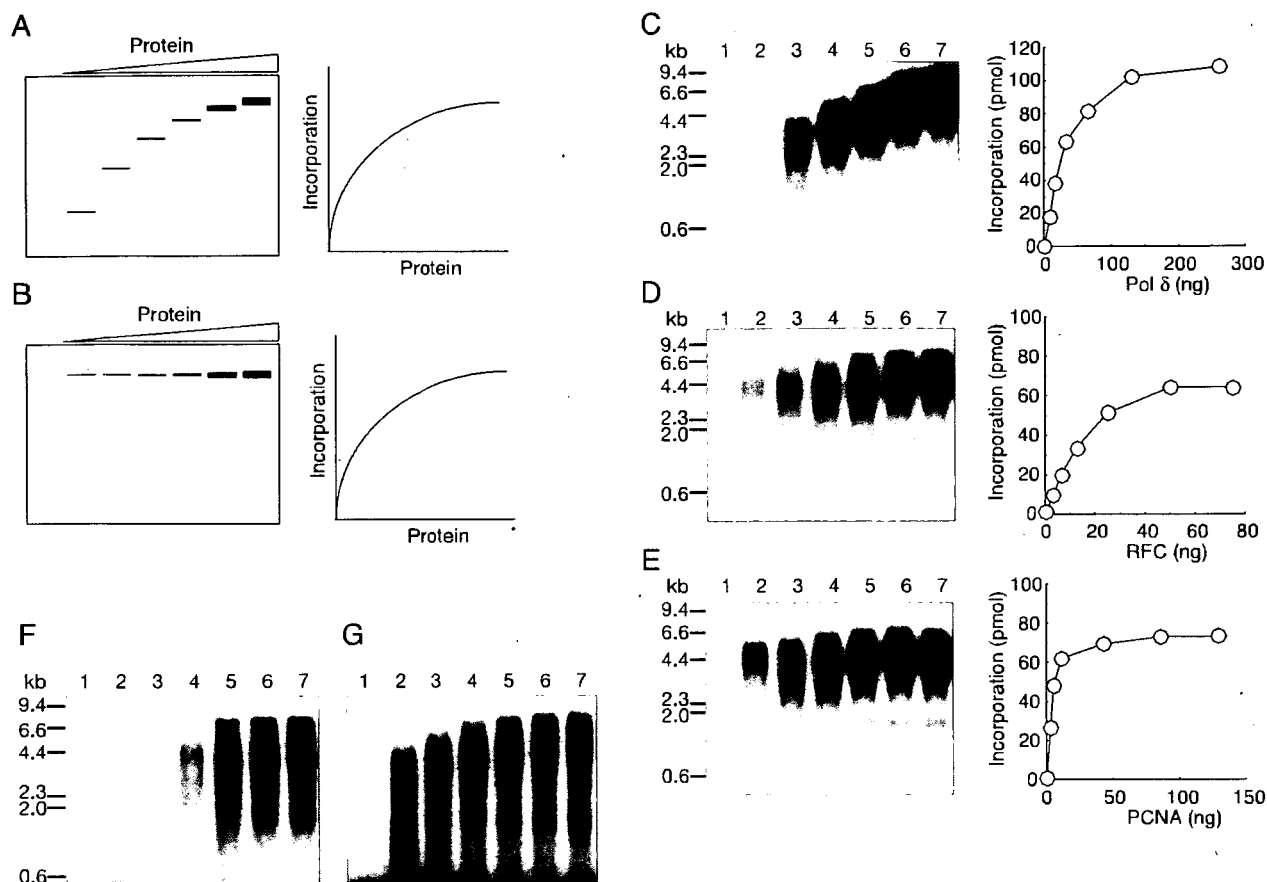


**Figure 2.** Analysis of the modes of action of replication factors in ss mp18 DNA replication. (A and B) Expected results of titration of a distributive factor (A) or a processive factor (B) on the DNA replication. The left panels represent gel images of alkaline-agarose gel electrophoresis, and the right panels represent graphs of quantified data for reaction products. See the text for details. (C–E) Titration of replication factors, pol  $\delta$  (C), RFC (D) and PCNA (E). Reactions were carried out for 10 min under the conditions described in the Materials and Methods section except for variation in the amounts of single protein factors. Reaction products were analyzed by 0.7% alkaline-agarose gel electrophoresis and the newly synthesized DNA were visualized by the incorporated [ $\alpha$ - $^{32}$ P]dTMP (left panels). Incorporation of dNMP were measured as described in the Materials and Methods' section (right panels). Titration of pol  $\delta$  (C); 0 ng (lane 1), 8.1 ng (lane 2), 16 ng (lane 3), 33 ng (lane 4), 65 ng (lane 5), 130 ng (lane 6) and 260 ng (lane 7). Titration of RFC (D); 0 ng (lane 1), 3.1 ng (lane 2), 6.3 ng (lane 3), 13 ng (lane 4), 25 ng (lane 5), 50 ng (lane 6) and 75 ng (lane 7). Titration of PCNA (E); 0 ng (lane 1), 2.7 ng (lane 2), 5.4 ng (lane 3), 11 ng (lane 4), 43 ng (lane 5), 86 ng (lane 6) and 129 ng (lane 7). (F and G) Titration of RFC (F) and PCNA (G) in the reactions using the  $5'$ - $^{32}$ P-labeled primer. The labeled primer was annealed to ss mp18 DNA, and [ $\alpha$ - $^{32}$ P] dTTP was replaced with cold dTTP in the reaction mixtures. Amounts of proteins used in the titration were the same as for D and E.

caused by the secondary template structure (35). Therefore, we conclude that pol  $\delta$  is not completely processive in this assay system.

Next, we changed concentrations of RFC (Figure 2D). The result was different from the case of pol  $\delta$ . Essentially, the concentration of RFC affected only the amount of products, but not their size (Figure 2D) (6,37), although increase of size at higher concentrations of RFC was noted (Figure 2D, lanes 6 and 7). The processive nature of RFC might be explained in two alternative ways. One is that the sole role of RFC is loading of PCNA at the initiation step (38). Once PCNA is loaded, due to stable association with DNA, RFC may no longer be required. If so, even after dissociation of pol  $\delta$  from the growing  $3'$ -hydroxyl end, once loaded PCNA may remain at the primer terminus and assist reassociation of pol  $\delta$ . The other explanation is that once RFC binds to a primer end

and loads PCNA to DNA, it may travel with PCNA and pol  $\delta$  (26,39,40). In the latter case, after dissociation of pol  $\delta$ , RFC may continue to hold PCNA at the primer terminus, and if the RFC unloaded PCNA (41–43) or if PCNA slide out of the primer terminus (44), the remaining RFC could reload PCNA quickly from solution. Therefore, it seems to be a very critical question, how the concentration of PCNA affects the size of the products. If PCNA behaves as a processive factor, RFC should be required only for the initiation step to load PCNA. On the other hand, if PCNA behaves as a distributive factor, then RFC would have to be traveling with growing  $3'$ -hydroxyl ends as a processive factor for loading PCNA anytime during elongation.

Thus, we subsequently examined effects of varying PCNA concentrations on the product size distribution. When the concentrations of PCNA were low, sizes of the

products became slightly decreased and smears <2 kb appeared (Figure 2E, lanes 2–4). However, large products (4–5 kb) were also detected, even at the lowest concentration of PCNA (Figure 2E, lane 2). In these assays, full-size products are excessively represented by their greater incorporation of radioactive nucleotides. To avoid this problem, we used a 5'-<sup>32</sup>P-labeled primer. Note that the size distribution of the products in the PCNA titration, different from that in RFC titration, was more clearly visualized with a 5'-<sup>32</sup>P-labeled primer than with incorporation of [ $\alpha$ -<sup>32</sup>P]dTMP (Figure 2F and G). The results revealed that the concentration of PCNA did not affect the initiation step, because the amount of utilized primer was not appreciably decreased with lower concentrations of PCNA (Figure 2G). On the other hand, the initiation was limited at a low concentration of RFC (Figure 2F), suggesting inefficient turnover of RFC. We consider that after dissociation of pol  $\delta$  from the growing 3'-hydroxyl end, some PCNA does not remain at the primer terminus, rather sliding out or being unloaded by RFC. In both cases, another PCNA might be reloaded from solution. Therefore, the results suggested that PCNA is partially distributive in our assay system, and also suggested that the processive nature of RFC is due to a stable association at the primer terminus during elongation of DNA replication. These issues were addressed intensively in subsequent experiments.

#### DNA replication on linearized ss mp18 DNA

For further analysis of PCNA and RFC actions during elongation, we examined the effects of linearization of mp18 DNA after initiation of DNA replication by introduction of a restriction enzyme, HincII, into reaction mixtures (Figure 3). A unique cutting site of HincII in the template DNA is located 29-bases downstream from the 3'-hydroxyl end of the primer. Soon after initiation of DNA replication, the region should be converted to double-stranded DNA and become cleavable by HincII (Figure 3A). In standard reaction mixtures, we introduced 10 U of HincII that can digest more than 98% of double-stranded mp18 DNA, for 15 s. As shown in Figure 3B, the sizes of all the products became uniformly much shorter in the presence of HincII and incorporation of dNMP was decreased by half (Figure 3B), probably due to a defect in elongation, rather than initiation, because the average size of products was also reduced by almost a half (Figure 3B). We considered that the decreased efficiency of DNA synthesis was probably the consequence of dissociation of PCNA, suggesting that some PCNA once assembled into the elongation complex might not remain at primer termini during elongation, and with a circular template, the majority of detached PCNA slides back to be reutilized.

The results shown in Figure 2 suggest that RFC remains at growing 3'-hydroxyl ends and reloads PCNA from solution during elongation. This implies that DNA synthesis can be resumed again after PCNA is once dissociated from the primer termini. If this were indeed the case, the size of the products should increase in a time-dependent manner. The results shown in Figure 3C

indicate that incorporation increased and the products became longer depending on the incubation time, but with a slower rate, suggesting reloading of PCNA from solution. Because pausing likely promotes the dissociation of pol  $\delta$  from PCNA (35), some PCNA also would be released from the primer termini at pausing sites. As expected these became more prominent, resulting in a more heterogeneous size distribution of products (Figure 3C).

Then, we further tested whether the concentration of RFC could affect the size of products in the presence of HincII (Figure 3D). Again, only the amount, but not the size distribution, was affected, although increase of the size at higher concentrations of RFC was observed, as in the reaction without HincII (Figure 2D). In contrast, the concentration of PCNA partially affected the size distribution of products (Figure 3E). The difference between RFC and PCNA titration was not clear by visualization with incorporation of the radioactive nucleotides. However, the 5'-<sup>32</sup>P-labeled primer, as shown in Figure 2F and G, was unavailable because of the restriction cutting. To solve the problem, newly synthesized strands were visualized, instead, by Southern hybridization with an oligonucleotide annealed to the newly synthesized strand just downstream of the HincII site. Results confirmed the difference in size distributions of the products between in the PCNA titration and RFC titration (Figure 3F and G). Since some PCNA slides out of the DNA (Figure 3B) and is reloaded from solution many times by RFC to continue DNA synthesis (Figure 3C), the size of the products would depend on the concentration of RFC, if this acted distributively. Therefore, our results again suggested that RFC acts processively, binding in the initiation of DNA replication and traveling with pol  $\delta$ .

#### Inefficient elongation by spontaneous loading of PCNA from template DNA ends

It is known that PCNA is spontaneously loaded from a double-stranded end of template DNA in an RFC-independent manner, and supports elongation with pol  $\delta$  (44). Therefore, the restart reactions after dissociation of PCNA observed in Figure 3C could be due to spontaneous loading of PCNA at the ends. To determine the efficiency of RFC-independent restart, ss mp18 DNA was linearized first, then subjected to reactions in the absence of RFC. In this assay, a primer covering HincII site was annealed to ss mp18 DNA (Figure 4A). HincII was introduced in standard reaction mixtures, and then the reactions were started by addition of pol  $\delta$  after preincubation for 1 min (Figure 4A). The time course of the reaction revealed the extension rate to be much slower (Figure 4B) than that of RFC-dependent reactions (Figure 3C) and the primer ends were hardly extended beyond the pausing site around 4 kb (Figure 4B). Next, we examined effects of varying PCNA concentrations on the size distribution of the products. The results demonstrated that the length of the products is uniformly short at a low concentration of PCNA (Figure 4C), suggesting that PCNA once assembled with pol  $\delta$  is not stable

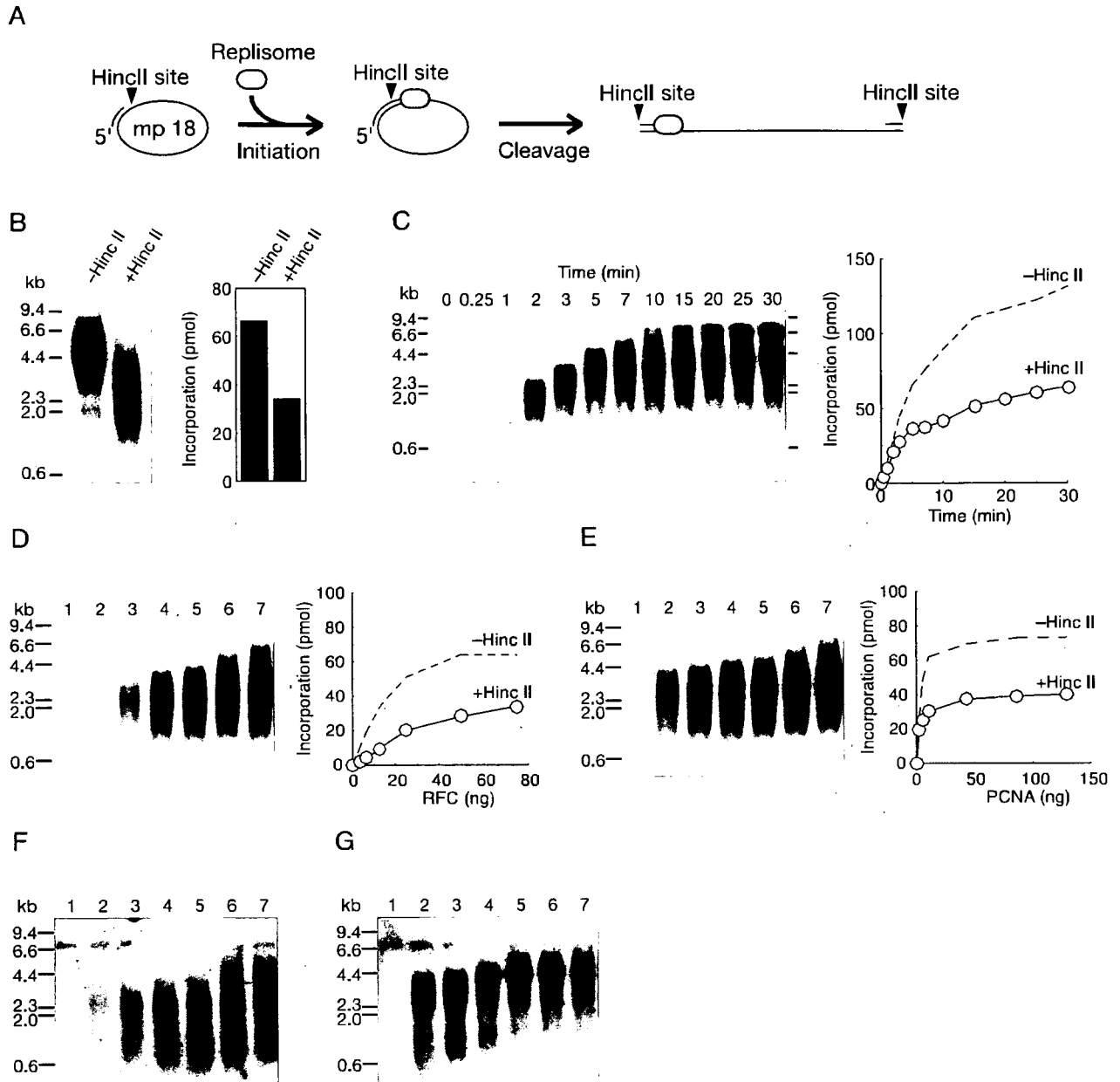


**Figure 3.** Effects of linearization of newly synthesized DNA just after initiation of DNA replication. (A) Schematic representation of the experimental design. A restriction enzyme, HincII, was introduced into the reaction mixtures. A unique cutting site in the template DNA is located 29-bases downstream from the 3'-hydroxyl end of the primer. After the region was converted to double-stranded DNA by initiation of DNA synthesis, indicating assembly of elongation complexes, the DNA becomes cleavable by HincII. (B) Effects of HincII on synthesis of ss mp18 DNA. (C) Time course of DNA synthesis in the presence of HincII. (D and E) Titration of RFC (D) and PCNA (E) in the presence of HincII. Amounts of PCNA and RFC used in the titration were the same as used for Figure 2 (see legend of Figure 2). Autoradiograms of 0.7% alkaline-agarose gels (left panels) in which the newly synthesized DNA was visualized by the incorporated [ $\alpha$ - $^{32}$ P]dTTP, and incorporation of dNMP were measured as described in the Materials and Methods section (right panels). Dotted lines represent results without HincII of Figure 2B. (F and G) Titration of RFC (F) and PCNA (G) in the presence of HincII. [ $\alpha$ - $^{32}$ P] dTTP was replaced with cold dTTP in the reaction mixtures and the newly synthesized strands were visualized by Southern blotting with a 5'-labeled oligonucleotide, which is complementary to newly synthesized strand just downstream of HincII site. Amounts of proteins used in the titration were the same as for (D) and (E). Reactions in (B, D-G) were carried out for 10 min under the conditions described in the Materials and Methods section with addition of HincII (10 U/25  $\mu$ l of reaction mixture).

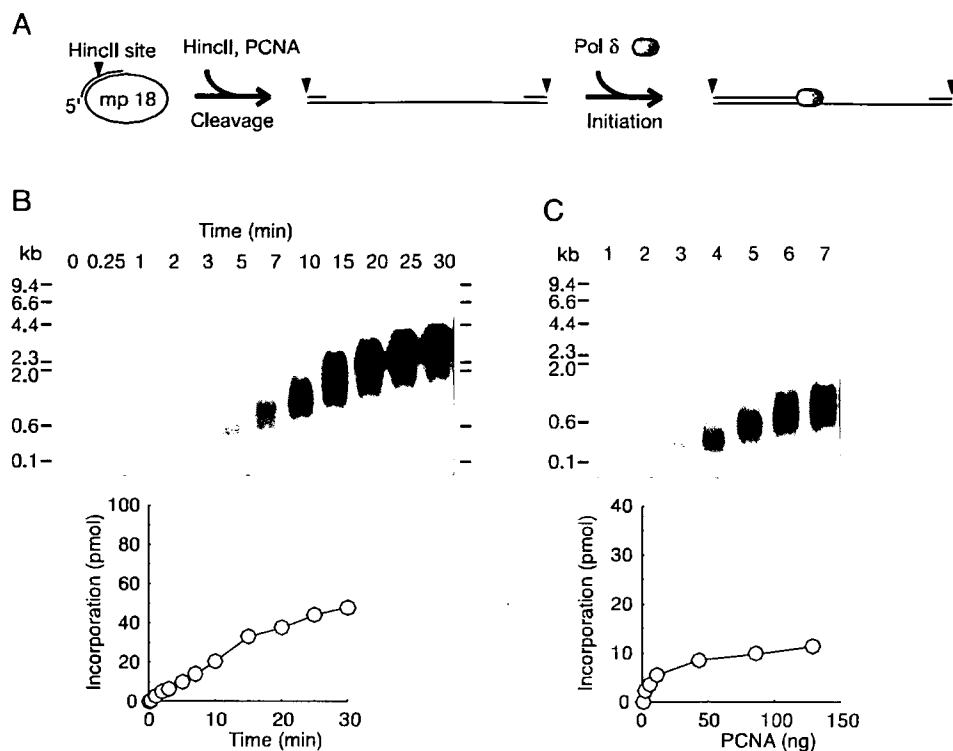


**Figure 4.** Effect of PCNA loaded spontaneously at ends of template DNA. (A) Schematic representation of the experimental design. A primer that covered HincII site was annealed to ss mp18 DNA. HincII (10 U) was introduced into standard reaction mixtures (25  $\mu$ l) under the conditions described in the Materials and Methods section except for omitting RFC. After pre-incubation for 1 min, reactions were started by addition of pol  $\delta$ . (B) Time course of DNA synthesis in the absence of RFC. (C) Titration of PCNA in the reactions without RFC. Amounts of PCNA used in the titration were the same as for Figure 2 (see legend of Figure 2). Reactions were carried out for 10 min. Autoradiograms of 0.7% alkaline-agarose gels in which the newly synthesized DNA were visualized by the incorporated  $[\alpha\text{-}^{32}\text{P}]\text{dTTP}$ , and incorporation of dNMP were measured as described in the Materials and Methods section.

during elongation. These results revealed differences between RFC-dependent and -independent reactions, indicating a requirement of RFC for efficient restart after dissociation of PCNA on linearized DNA.

#### Effects of dilution of the elongation complexes

A different method of analysis was used to investigate the action of protein factors. Here, after the replication complex was assembled, the reaction mixture containing the complexes was diluted in pre-warmed reaction mixtures containing all the protein components at the same concentration, except one component. As with the previously described method, if the protein in question acts distributively, one would expect to observe a shift to shorter products with diluted reaction mixtures (32).

As schematically shown in Figure 5A, the primer-template DNA was mixed with saturating concentrations of RPA, PCNA and RFC, and then 1 min later pol  $\delta$  was added for formation of replication complexes. At 15 s after the initiation complex was presumably assembled, an aliquot of the reaction mixture was diluted 10-fold either into a pre-warmed reaction mixture containing all the auxiliary proteins and pol  $\delta$ , or into a similar one omitting one or two of PCNA, RFC and pol  $\delta$  (Figure 5A). Then, reactions were continued for further 10 min, and the

products were analyzed by alkaline-agarose gel electrophoresis (Figure 5B). Dilution of either PCNA or pol  $\delta$  resulted in a decrease in the size of the products (Figure 5B, lanes 2 and 4) as compared to the complete case (Figure 5B, lane 1). This effect was more pronounced when both PCNA and pol  $\delta$  were diluted together (Figure 5B, lane 7); virtually no products were detected. On the other hand, dilution of RFC exerted no influence (compare lanes 1 and 3 in Figure 5B). Furthermore, when both PCNA and RFC were diluted together, the size distribution of products was almost identical to that with dilution of PCNA alone (compare lanes 2 and 5 in Figure 5B). These results indicated that PCNA and pol  $\delta$  are supplied from solution, whereas RFC is not, during the elongation. Furthermore, we noted that when both RFC and pol  $\delta$  were diluted together, the product size was decreased to a much greater extent than with dilution of pol  $\delta$  alone (compare lanes 4 and 6 in Figure 5B). This suggested that when reassociation of pol  $\delta$  is limited, RFC is needed from solution. The importance of this observation is discussed below.

We also tested if adenosine (3-thiotriphosphate) (ATP $\gamma$ S) affected elongation reactions. When ATP in the dilution mixture was replaced with ATP $\gamma$ S, elongation reactions were completely halted (Figure 5B, lane 9).

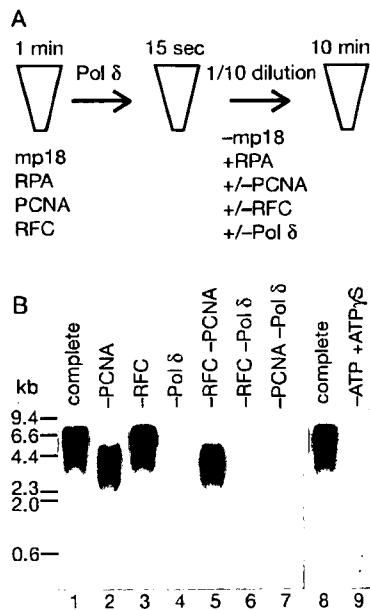


**Figure 5.** Effects on size distribution after dilution of elongation complexes. (A) Outline of the assay. At 15 s after the reaction was started by addition of pol  $\delta$  under standard reaction conditions described in the Materials and methods section, 10-fold dilution was performed with pre-warmed reaction mixtures without template but containing all the protein components or omitting one or two of them. Both reaction mixtures, before and after dilution, contained [ $\alpha$ - $^{32}$ P]dTTP. After a further 10 min incubation, the reaction products were analyzed by 0.7% alkaline-agarose gel electrophoresis. (B) An autoradiogram of a 0.7% alkaline-agarose gel. The indicated proteins were omitted in the dilution mixtures. In the reaction shown in lane 9, 1 mM ATP in the dilution mixture was replaced with 2.5 mM ATP $\gamma$ S.

This suggested that the ATPase activity of RFC is required for the elongation phase of replication (24), consistent with our assumption that RFC remains around primer terminus, and holds, unloads and reloads PCNA.

#### Functions of the POLD3 subunit of pol $\delta$

The role of the 66 kDa subunit, POLD3, of pol  $\delta$  in the dynamic processes involved in elongation, and the biochemical properties of subassembly (pol  $\delta^*$ ) lacking the POLD3 subunit are of great interest. First, we examined the efficiency of DNA synthesis of human pol  $\delta^*$  using purified proteins (Figure 6A). A comparison of activities with equivalent amounts of pol  $\delta^*$  and pol  $\delta$  demonstrated inefficiency of pol  $\delta^*$  under the standard reaction conditions with singly primed ss mp18 DNA (Figure 6B), decrease and heterogeneity in length of the products being observed with emphasized pausing sites (Figure 6B and C). The shorter products were shifted to longer ones at higher concentrations of pol  $\delta^*$  (Figure 6C), as with pol  $\delta$  (Figure 2C). When the missing subunit, POLD3, was introduced into the reaction with pol  $\delta^*$ , the activity was restored to the level with pol  $\delta$  (Figure 6B), indicating that the lower activity of pol  $\delta^*$  was due to the missing function of POLD3 subunit, rather than denaturation of proteins caused by incomplete assembly.

The evidence presented here is consistent with reports for yeast counterparts (30,45) and human pol  $\delta$  (36,46).

Next, we tested whether variation in the concentrations of RFC and PCNA might affect the size of products in reactions with pol  $\delta^*$ . RFC was without influence, again suggesting stable association (Figure 6D). In contrast, the size of products varied with the concentration of PCNA (Figure 6E), in line with a requirement for a continuous supply of PCNA from solution for efficient DNA synthesis. Notably, with low concentrations of PCNA, all the products were uniformly small in reactions with pol  $\delta^*$ , exhibiting an entirely distributive nature. Furthermore, we tested the effect of linearization on mp18 DNA after initiation of DNA replication by addition of HincII (Figure 6F). DNA synthesis with pol  $\delta^*$  was very sensitive to linearization of DNA, and increasing concentrations of PCNA slightly restored the defect (Figure 6F). However, the majority of intermediates on elongation could not overcome the first pausing site (around 0.6–1 kb), even at the highest concentration of PCNA (Figure 6F). These results suggested frequent dissociation of PCNA during elongation with pol  $\delta^*$ .

#### Amounts of PCNA loaded on mp18 DNA during elongation

Since an excess PCNA was required for efficient DNA synthesis with pol  $\delta^*$  (Figure 6E), we considered whether PCNA might accumulate on DNA during elongation. If so, the frequency of sliding back to the primer terminus would increase and an increase in the local concentration of PCNA would help interactions with pol  $\delta^*$  at the primer terminus. To measure the amount of PCNA loaded on DNA directly, a primer containing an extended 5' tail with one biotin molecule was annealed to ss mp18 DNA (Figure 7A). The primed ss mp18 DNA was then attached to magnetic beads and DNA replication reactions were carried out under standard reaction conditions (Figure 7A). The 5' tail did not exert any influence on DNA synthesis (data not shown). In the reactions, 33 ng of pol  $\delta$  and 140 ng of pol  $\delta^*$  were used since these amounts lead to equivalent efficiency of DNA synthesis ( $\sim$ 40 pmol of the incorporation of dNMP) and to the same size distribution of products (compare lane 3 of Figure 2C with lane 7 of Figure 6C). After reactions for 10 min, PCNA bound to beads was detected by western analysis (Figure 7B). In this assay, non-specific association of PCNA with beads or DNA was detected (Figure 7B, lane 2). When RFC was introduced into the reaction, an increase of binding of PCNA was observed. The increased amount of PCNA (difference between lanes 2 and 3 in Figure 7B) was 40 fmol, which was equivalent to that of primer template (33 fmol), suggesting specific loading to the primer terminus. Introduction of pol  $\delta$  increased the amount of PCNA only slightly (Figure 7B, lane 4). The majority of PCNA was dissociated by introduction of HincII with a decreasing signal to background level (Figure 7B, lane 5), again indicating specific loading on the DNA. When pol  $\delta^*$  was used instead of pol  $\delta$ , excessive accumulation of PCNA was unexpectedly not observed (Figure 7B, lane 6), suggesting that we cannot attribute the entire distributive nature of PCNA on the